JOURNAL OF GEOPHYSICAL RESEARCH, VOL. 99, NO. B10, PAGES 20,095–20,122, OCTOBER 10, 1994

The Teton fault, Wyoming: Topographic signature, neotectonics, and mechanisms of deformation

John O. D. Byrd[1] and Robert B. Smith
Department of Geology and Geophysics, University of Utah, Salt Lake City

John W. Geissman
Department of Earth and Planetary Sciences, University of New Mexico, Albuquerque

Abstract. We integrated geophysical and geological methods to evaluate the structural evolution of the active Teton normal fault, Wyoming, and its role in the development of the dramatic topography of Teton Range and Jackson Hole. The Teton fault bounds the precipitous eastern front of the Teton Range and is marked by large, well-preserved postglacial fault scarps that extend for 55 km along the range front. Comparison of variations in surface offsets with the topographic expression of the Teton range crest and drainage divide, and the overall structure of the range, suggests that the effects of postglacial faulting cannot be discriminated from the influence of pre-extensional structures and differential erosion on the footwall topography. In contrast, the effects of multiple scarp-forming normal faulting earthquakes are expressed by the anomalous drainage pattern and westward tilt of the hanging wall, Jackson Hole, toward the Teton fault. Kinematic boundary element fault models suggest that the westward tilt of the valley floor is the product of 110-125 m of displacement on a 45°-75°E dipping Teton fault in the past 25,000-75,000 years. Comparisons with historic normal faulting earthquake displacements imply that this range of displacement corresponds to 10-50, $M > 7$ scarp-forming earthquakes. A total throw of 2.5 to 3.5 km across the Teton fault is suggested by inverse ray-tracing and forward gravity models. These models also suggest that Laramide age structures have been offset across the Teton fault and obscure its geophysical signature but also continue to influence the structural and topographic expression of the footwall and hanging wall blocks. Paleomagnetic analyses of the ~2.0 Ma Huckleberry Ridge Tuff suggest that the overall westward tilt of the Teton Range is a result of about 10° of west side down tilt across the Teton fault since tuff emplacement. This suggests that much if not all of the throw across the Teton fault has accumulated in the past 2 m.y. Complex demagnetization and rock magnetic behavior and local emplacement of the Huckleberry Ridge Tuff on preexisting topography preclude determination of the amount or variations in throw along strike of the Teton fault from the paleomagnetic data.

Introduction

The precipitous eastern range front and spectacular topography of the Teton Range and adjoining valley of Jackson Hole, Wyoming (Figure 1), are a manifestation of displacement across the active Teton normal fault. Well-preserved, 3-52 m high, Holocene fault scarps extend for 55 km along the range front, indicating that the Teton fault was the locus of several large ground-rupturing normal faulting earthquakes in the past 17,000 years [*Susong et al.*, 1987; *Smith et al.*, 1990, 1993a; *Byrd*, 1994]. (Throughout this paper all references to postglacial, Pinedale ages are in calendar years and have been converted from ^{14}C years using the calibration of *Stuiver and Reimer* [1993].) In spite of this evidence for extensive postglacial faulting, the historic seismic record suggests that the Teton fault occupies a zone of seismic quiescence in the Intermountain Seismic Belt at the $M > 3$ level [*Smith et al.*, 1990, 1993a; *Smith and Arabasz*, 1991].

The Teton fault extends for up to 70 km along the base of the Teton Range and is located near the junction of four major tectonic provinces: the Basin and Range, Idaho-Wyoming thrust belt, Rocky Mountain Foreland, and Snake River Plain-Yellowstone volcanic plateau (Plate 1 and Figure 2). The average N10°E fault strike is oblique to the dominant NW-SE structural grain of both the Late Cretaceous to early Tertiary contractional and Basin and Range extensional structures (Figure 2). The apparent southern termination of the fault near Mesozoic to early Tertiary thrusts suggests that these preexisting structures may influence its lateral extent.

The eastward dip of the Teton fault and corresponding eastward facing Teton mountain front are relatively anomalous in the northeastern Basin and Range province (Figure 2). Estimates of maximum throw across the fault range from 2.1 to 11 km (Table 1). Structural relief across the fault decreases from at least several kilometers to less than 500 m over a distance of 15 km along strike. The decrease in structural relief is reflected by the lower elevations of the range crest to the north

[1] Now at Exxon Production Research Company, Houston, Texas.

Paper number 94JB00281.
0148-0227/94/94JB-00281$05.00

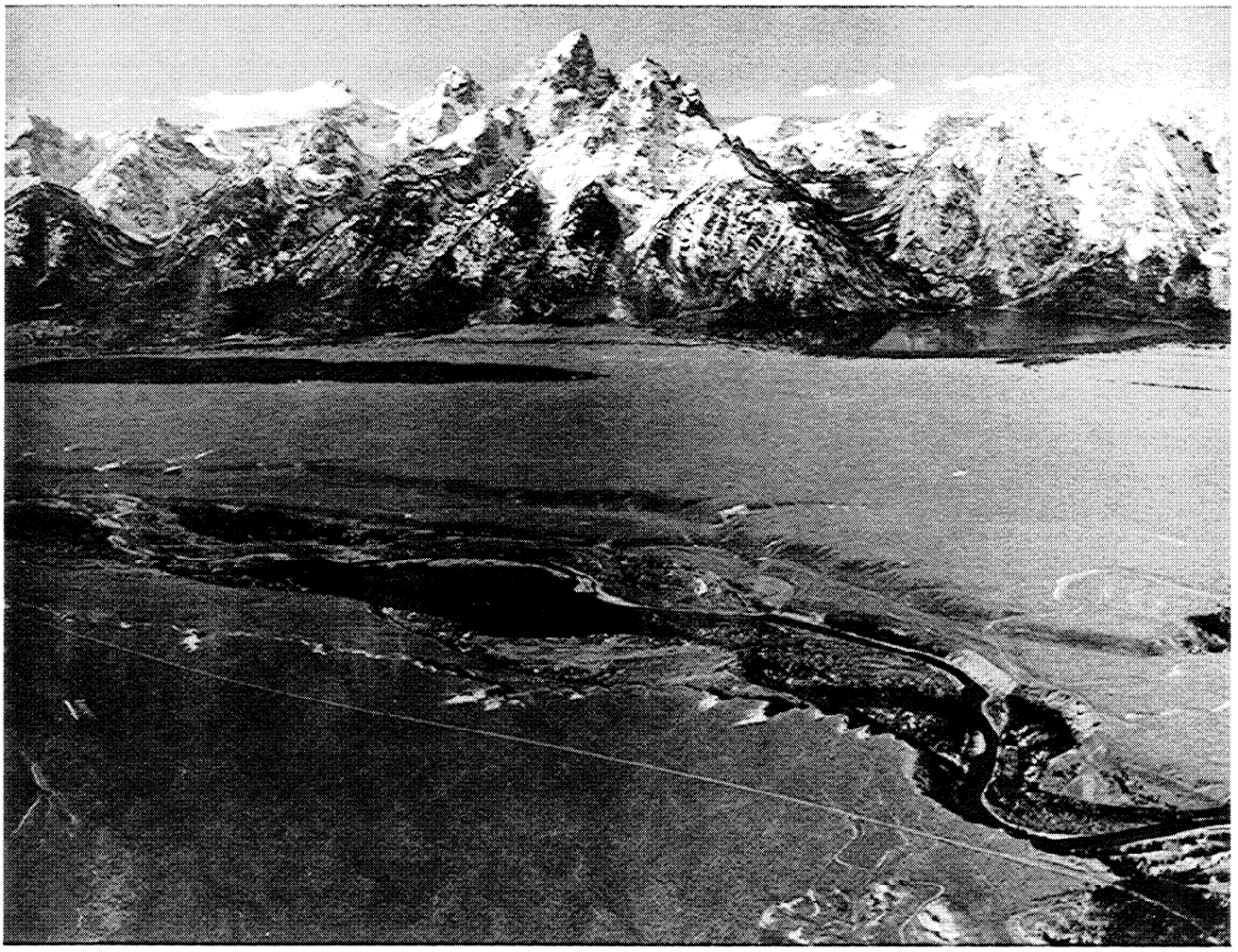

Figure 1. View of the precipitous eastern front of the Teton Range and spectacular topography of the Grand Teton (4067 m) and other peaks of the Cathedral Group to the right. Timbered Island, a Bull Lake glacial moraine, is the tree-covered dark area east of the mountain front on the left side of the picture. The Snake River and related terraces cross the lower part of the picture. Photograph provided courtesy of D.R. Lageson.

and south away from the high peaks in the central part of the Teton Range (Plate 1 and Figure 1).

This paper summarizes the structural evolution of the Teton fault and its role in shaping the topographic expression of the Teton area. We have integrated geophysical and geological studies of a series of overlapping spatial and temporal reference frames, and present (1) implications of footwall and hanging wall topography on overall variations in fault displacement; (2) results of detailed topographic surveys across the hanging wall coupled with boundary element fault modeling to determine post-75,000-25,000-year fault displacement and subsurface fault geometry; (3) seismic refraction and gravity data modeling to evaluate total fault displacement, subsurface fault and hanging wall geometry; and (4) paleomagnetic data from the ~2.0 Ma Huckleberry Ridge Tuff to evaluate the pre-Quaternary topographic expression of the Teton Range and its post-Quaternary deformation. We integrate these results with our detailed fault mapping [*Susong et al.*, 1987; *Smith et al.*, 1993a], paleoseismological [*Byrd*, 1991; *Byrd*, 1994], geodetic [*Sylvester et al.*, 1991; J.O.D. Byrd et al., Geodetic evidence for aseismic deformation across the Teton fault, submitted to Journal of Geophysical Research, 1994], and geochemical and geochronological studies (J.O.D. Byrd et al., manuscript in preparation, 1994), and other published work to summarize our understanding of the neotectonics of the Teton fault.

Tectonic History and Previous Work

The Teton Range is the product of a diverse tectonic history. The core of the range consists of Precambrian metamorphic and plutonic rocks unconformably capped by west-dipping Paleozoic strata [e.g., *Reed and Zartman*, 1973, *Love et al.*, 1992]. Exposures of Mesozoic and lower Tertiary age strata are limited to relatively minor outcrops at the northern end of the range [*Christiansen et al.*, 1978]. Mesozoic to early Tertiary crustal shortening uplifted and folded these rocks forming the Laramide Teton-Gros Ventre uplift [e.g., *Blackwelder*, 1915; *Horberg et al.*, 1955; *Love et al.*, 1973; *Lageson*, 1992]. Results of fission track studies [*Roberts and Burbank*, 1993] suggest that the Precambrian and Cambrian rocks that made up the Teton-Gros Ventre uplift underwent 1-1.5 km of relative uplift between 85 and 65 Ma and approximately 2 km of additional uplift, or exhumation, have occurred since 30 Ma.

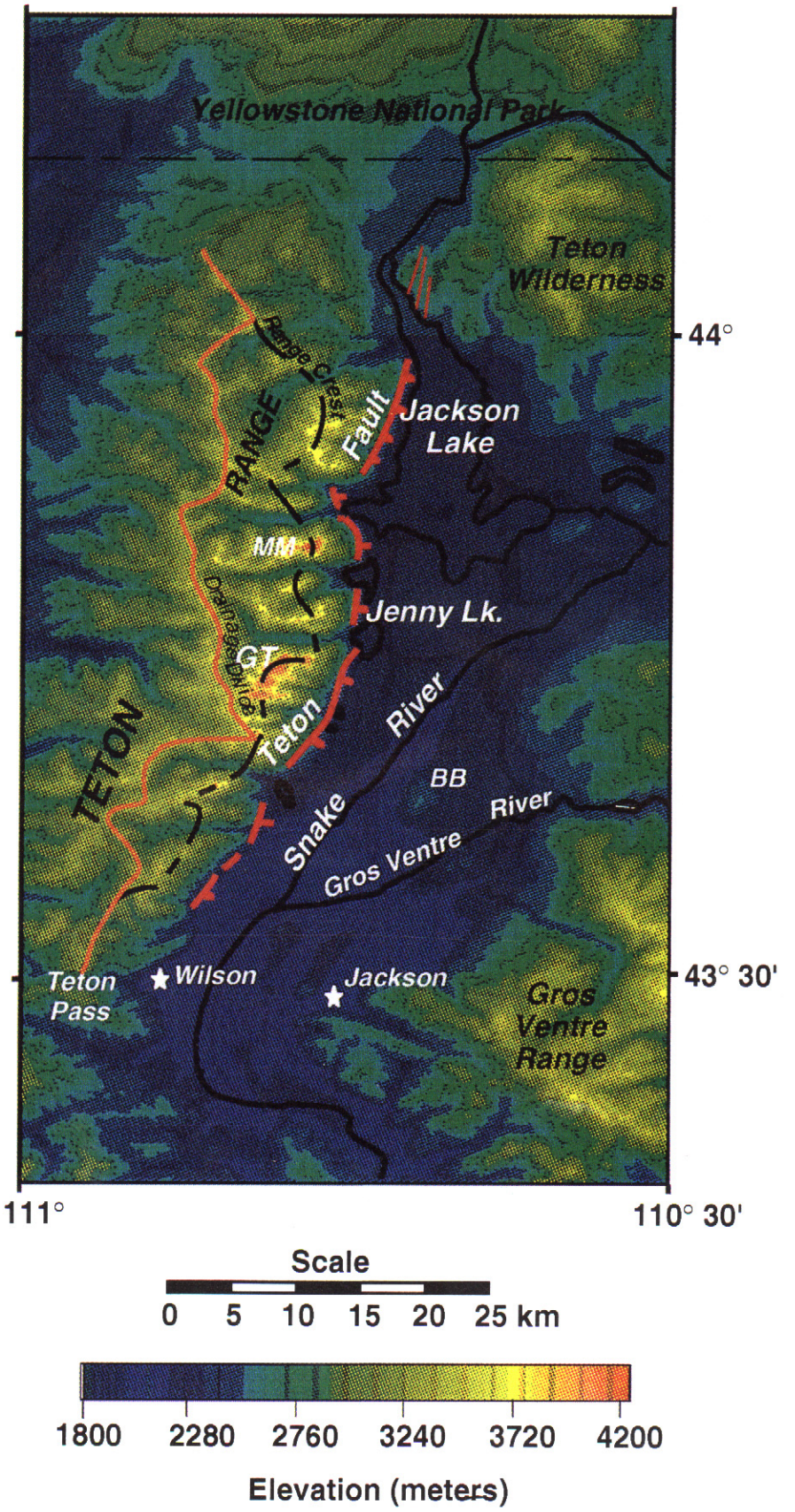

Plate 1. Contoured topographic map of the Teton-Jackson Hole area showing the Teton fault and locations cited in the text. Topographic data are from 1-km digital elevation model (DEM). BB, Blacktail Butte; GVB, Gros Ventre Buttes; GT, Grand Teton; MM, Mount Moran.

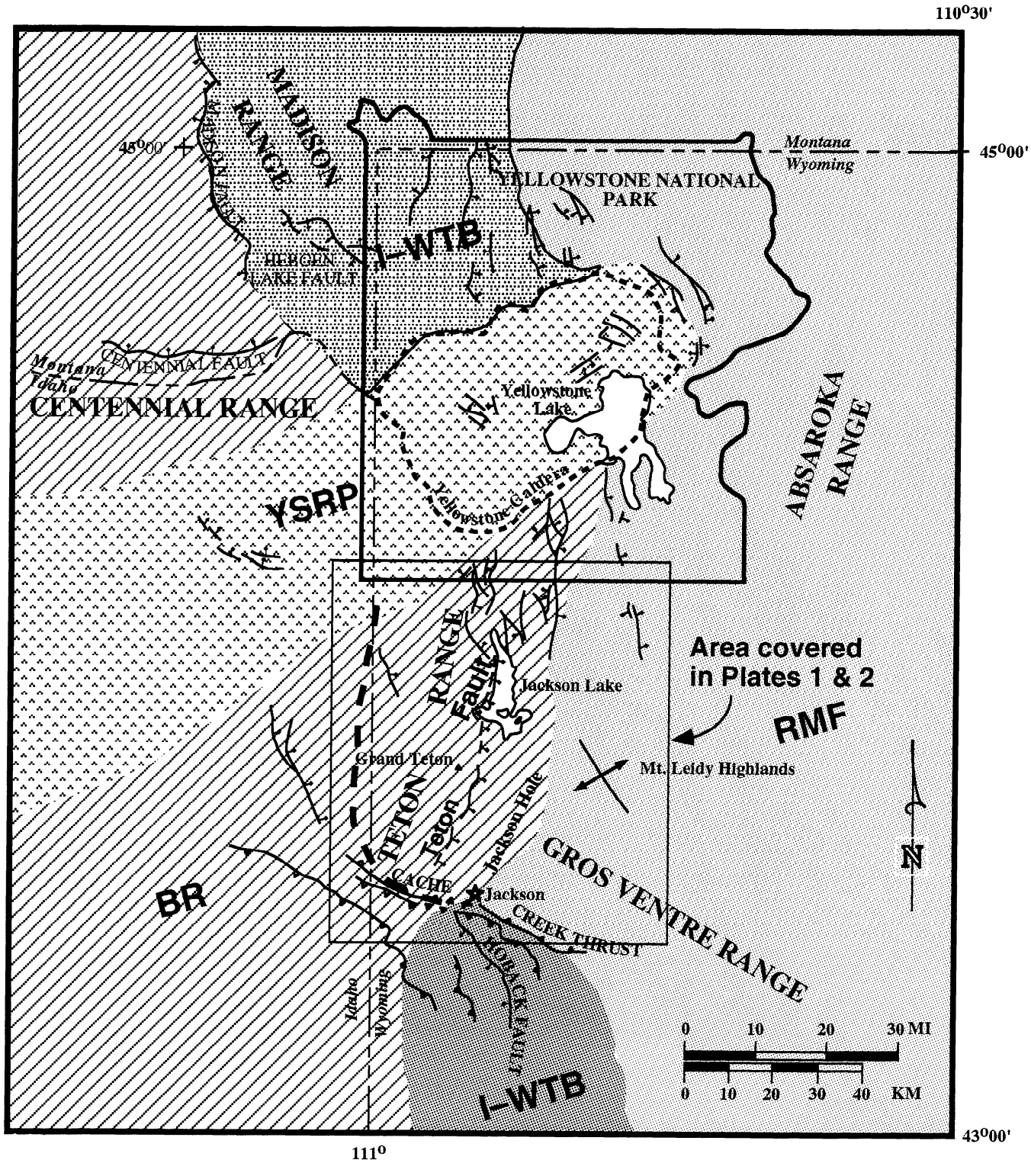

Figure 2. Simplified tectonic map of the Teton-Jackson Hole area showing location of the Teton fault and regional geologic features.

Superposition of Basin and Range epeirogeny, manifested by displacement on the Teton normal fault, subsequently dissected and offset of the Laramide-uplift [e.g., *Love et al.*, 1992]. Concomitant silicic volcanism, crustal uplift and subsidence associated with the Yellowstone-Snake River Plain volcanic system are manifested by deposition of late Miocene to Quaternary volcaniclastic rocks that unconformably overlie the older strata in the Teton Range. *Roberts and Burbank* [1993] suggested that late Tertiary, principally post-2 Ma, displacement on the Teton fault uplifted and tilted these younger strata and the entire Teton Range.

Miocene to recent lacustrine, volcaniclastic, glacial, fluvial and alluvial deposits blanket the valley floor of Jackson Hole [e.g., *Love et al.*, 1973]. A relatively continuous section of

Table 1. Estimated Displacements Across the Teton Fault

Investigator	Throw, km	Fault Dip	Age of Faulting	Criteria
Blackwelder [1915]	> 3		pre-Mid-Tertiary	physiographic, stratigraphic
Edmund [1951]	2.1 - 4.3	40° - 70°	Miocene-recent	stratigraphic and structural
Horberg et al. [1949]		> 45°	Miocene-recent	stratigraphic and structural
Fryxell et al. [1941]	2.4		post-Oligocene	stratigraphic, geomorphic
Horberg et al. [1955]		> 40°	Pliocene	stratigraphic offset
Lavin and Bonini [1957]	5 - 6	60° - 90°		gravity model
Behrendt et al. [1968]	7	30°-90°		gravity, seismic refraction
Tibbetts et al. [1969]	7	> 45°		seismic refraction model
Love and Reed [1971]	7.6-9.1		< 9 Ma	stratigraphic offset
Love et al. [1973]		85°		
Love [1977, 1987]	9-11		< 5 Ma	stratigraphic offset
Gilbert et al. [1983]	2.1-2.9	60° - 75°	< 5 - 6 Ma	Huckleberry Ridge Tuff
Barnosky [1984]			9.4-13 Ma	stratigraphic unconformity
Lageson [1992]		listric		regional structural features
Roberts and Burbank [1993]	3.5		< 28 Ma and < 2 Ma	fission track data
J.O.D. Byrd et al. (manuscript in preparation, 1994)	<10			fluid inclusion and $^{39}Ar/^{40}Ar$
This study	2.5 - 3.5	45°-75°		Gravity, seismic refraction, geodetic data, fault models

folded Paleozoic, Mesozoic, and Tertiary strata, representing the subsurface continuation of the Laramide-age Gros Ventre Range (Plate 2), is inferred to underlie these units [e.g., *Behrendt et al.*, 1968].

The Quaternary expression of the Teton fault was first noted by *Fryxell* [1938], who described displaced glacial features along the eastern range front. These postglacial fault scarps are preserved for 41 km of the 55 km Quaternary Teton fault trace (Plates 1 and 2 and Figure 3), near the contact between the Precambrian basement rocks and Holocene deposits [*Byrd* , 1994]. The discontinuity in fault scarps, accounting for the 14-km deficit, reflects the absence of fault exposures in areas of steep topography, lakes and landslides. A single, multiple-event fault scarp, 3-52 m high, displaying a down-to-the-east, normal sense of displacement in Pinedale glacial and younger fluvial and alluvial deposits typically marks the Teton fault trace [*Smith et al.*, 1990, 1993a; *Byrd*, 1994]. In the central part of the Teton fault, near Taggart Lake (Plate 1), offset moraine crests suggest left-oblique separation of 8-26 m. The inferred strike-slip component may account for up to 50% of the postglacial slip in this area; however, the complex geometry of intersecting nested glacial moraines makes this evidence for lateral offset equivocal. There is no evidence for similar horizontal displacements along the southern and northern parts of the fault where similar glacial features are offset vertically.

The northern part of the Teton fault trace is marked by a 1.5-km eastward step-over in the fault scarps north of Moran Bay (Plates 1 and 2). Fault scarps extend for 13 km along the base of the range front west of Jackson Lake until they intersect the northern lake shore. Northeast of Jackson Lake, the Teton fault is represented by a zone of both down-to-the-west and down-to-the-east normal faults (Plates 1 and 2) that offset Pinedale glacial deposits and the ~2.0 Ma Huckleberry Ridge Tuff [*Byrd*, 1991]. These normal faults are the southernmost expression of a right-stepping zone of normal faults that continues 30 km northeast into the Yellowstone Plateau.

On the basis of interpretations of gravity data and the distribution of outcrops of Paleozoic rocks east of the postglacial fault scarps, *Behrendt et al.* [1968], *Tibbetts et al.* [1969], *Gilbert et al.* [1983], and *Love et al.* [1992] concluded that the northern Teton fault extended beneath the west side of Jackson Lake. Seismic reflection and refraction profiles along the west side of the lake, however, revealed no evidence of significant displacement of the Quaternary lake deposits [*Smith et al.*, 1993b]. This apparent lack of displacement suggests that if faults are present beneath the west side and north end of Jackson Lake they have not ruptured the recent lacustrine sediments, and that postglacial displacements were restricted to the range front scarps. Alternatively, evidence of postglacial faulting may not have been preserved in the lake bottom sediments, or the deformation could not be resolved on the seismic profiles.

The postglacial expression of the southern part of the Teton fault ends on the north side of Phillips Canyon (Plate 1). The fault scarps in this area are exposed in glacial and colluvial deposits along the range front, 200 m above Fish Creek and the valley floor (Plate 1), and approximately 6 km north of the inferred location of the Late Cretaceous to early Tertiary Cache Creek and Jackson thrusts at the south end of Jackson Hole (Plate 2). A number of workers [*Love and Albee*, 1972; *Love et al.*, 1973; *Smith et al.*, 1977; *Doser and Smith*, 1983] proposed that the Teton fault is 90 km long, offsets the thrusts, and terminates in the hanging wall of the southwest-dipping Hoback normal fault (Figure 2). In contrast, *Sales* [1983], *Royse* [1983], and *Lageson* [1992] proposed that the Teton fault terminates at the Cache Creek thrust and soles into a north-northwest dipping thrust ramp at depth. Their interpretations suggest the Teton fault is hinged at its intersection with the Cache Creek thrust, requiring that the thrust act as a non-conservative barrier to rupture propagation along the Teton fault. Alternatively, the implied fault intersection may act as a nucleation point for ground-rupturing earthquakes on the Teton fault, suggesting that the Cache Creek thrust dips some 70°N if the earthquakes nucleated at 15 to 20 km depths.

The age of initiation of displacement on the Teton fault is controversial; estimates range from 13 Ma to as recently as 2 Ma, based on the angular unconformities between the Miocene Colter and Teewinott formations and Conant Creek Tuff exposed on the east side of Jackson Hole [*Barnosky*, 1984, *Love*

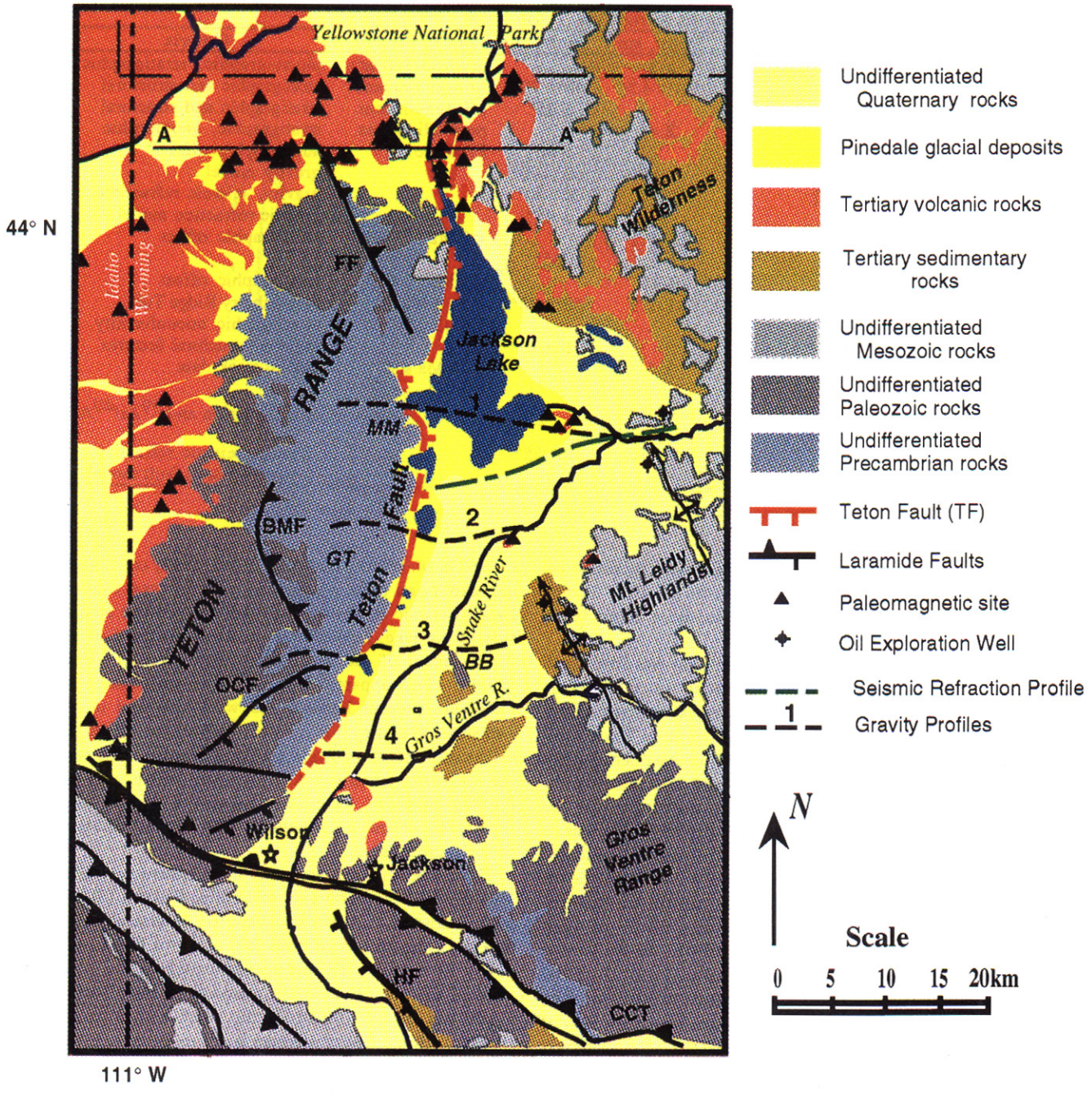

Plate 2. Simplified geologic map showing locations of paleomagnetic sampling sites, gravity profiles, and seismic refraction profile. Key geographic features discussed in text are also labeled. Line A-A' indicates location of geologic cross section illustrated in Figure 15. BMF, Buck Mountain fault; FF, Forellen fault; CCT, Cache Creek thrust; HF, Hoback fault; MM, Mt. Moran; OCF, Open Canyon fault; BB, Blacktail Butte. Geology is modified after *Love et al.* [1992] and Teton fault trace is from *Smith et al.* [1993a].

et al., 1992; *Smith et al.*, 1993b]. *Love* [1977] proposed that fault movement began at 5 Ma based on the lack of coarse clastic detritus in the lacustrine deposits of Teewinott Formation, 3 km east of the Teton range front. However, Quaternary to recent deposition of dominantly silt and clay size sediment adjacent to the mountain front and the Teton fault in Jackson Lake [*Shuey et al.*, 1977] tends to discount Love's stratigraphically based argument. Table 1 summarizes additional estimates of the age of inception of the Teton fault.

Estimates of the stratigraphic separation across the Teton fault range from 2.1 to 11 km (Table 1). The majority of these values range from 6 to 9 km and are based on stratigraphic arguments and reconstruction of the Paleozoic-Precambrian contact penetrated in oil exploration wells east of Jackson Hole and exposed at the top of Mount Moran (Plate 2) [e.g., *Behrendt et al.*, 1968]. Projections of the ~2.0 Ma Huckleberry Ridge Tuff, from exposures on Signal Mountain (Plate 2) westward beneath Jackson Hole, suggest that the tuff is present at depths of 2.1 to 3.0 km adjacent to the northern part of the Teton fault [*Gilbert et al.*, 1983; *Smith et al.*, 1993b]. *Gilbert*

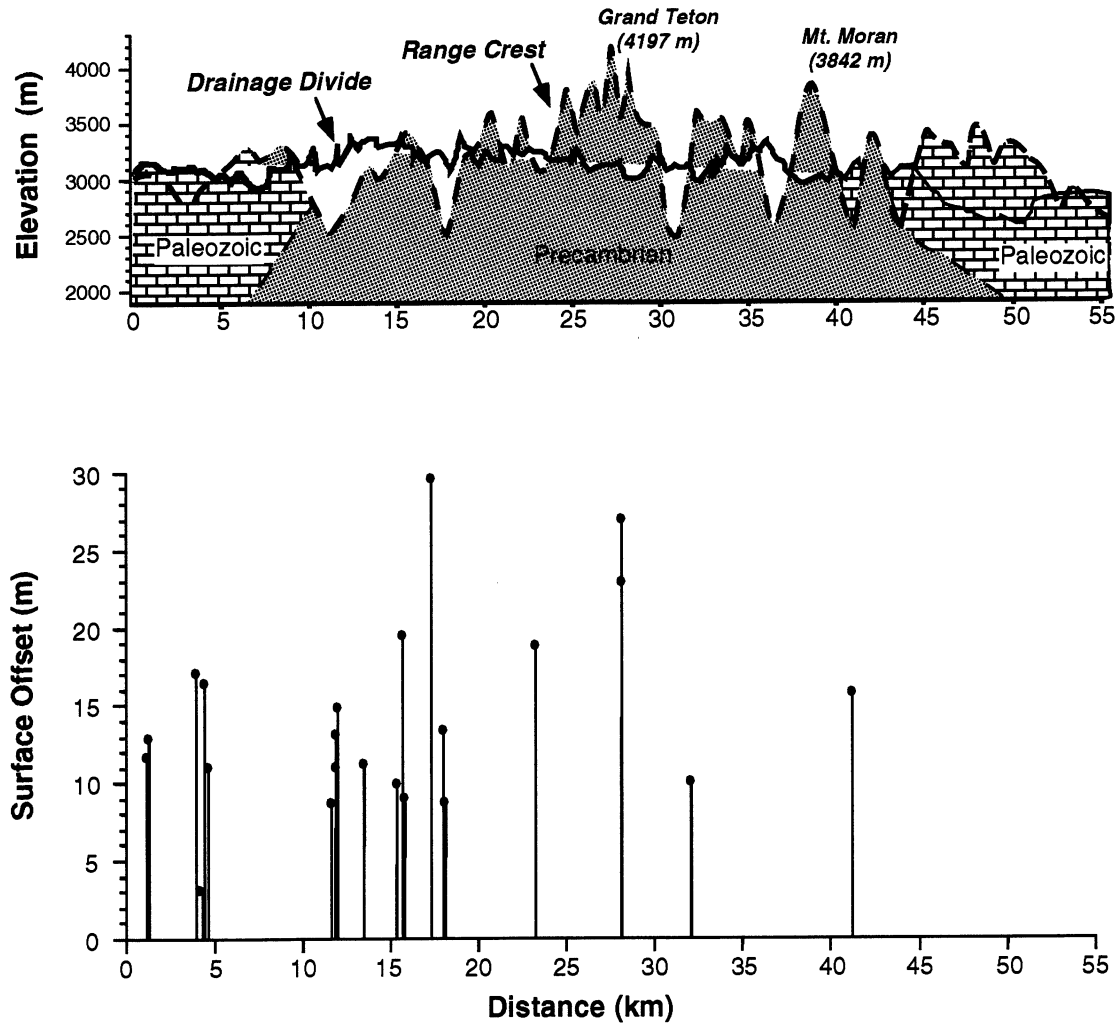

Figure 3. Plot showing drainage divide, range crest topography and surface offset across the Teton fault. (a) Topographic expression of the Teton range crest and drainage divide and generalized distribution of Paleozoic and Precambrian age rocks along each feature; and (b) postglacial surface offset along the Teton fault determined from fault scarp profiles [*Byrd,* 1994].

et al. [1983] interpreted this depth range as representing the total Quaternary throw on the fault, tacitly assuming that the Huckleberry Ridge Tuff was not emplaced as a continuous deposit covering the Teton Range and Jackson Hole.

Topographic Expression and Displacement on the Teton Fault

Uplift of the Teton Range along the Teton fault is exemplified by the westward tilt and overall topographic expression of the range as "a great block tilted along its eastern border" [*St. John,* 1879]. Concomitant hanging wall subsidence of Jackson Hole is manifested by the westward dip of the Miocene and younger formations exposed in the valley and anomalous westward tilt of the valley floor. The relationship between the topography of the range and post-2 Ma displacement on the Teton fault is discussed later in the context of the paleomagnetic analyses of the Huckleberry Ridge Tuff. In this section we focus on the effects of postglacial displacement on the Teton fault and the persistent influence of Laramide features on the topography of the Teton Range and Jackson Hole.

Seismotectonics of Normal Faults

The general relationship of footwall and hanging wall deformation produced by large normal-faulting earthquakes is exemplified by the surface deformation accompanying three well-studied, large earthquakes in the Basin and Range Province (Figure 4): the M_s = 6.8, 1954 Dixie Valley, Nevada, the M_s = 7.5, 1959 Hebgen Lake, Montana, and the M_s = 7.3, 1983 Borah Peak, Idaho earthquake [see *Smith and Arabasz,* 1991, and references therein]. These earthquakes nucleated at mid-crustal depths, 15 ± 5 km, on 45° to 60° dipping planar normal faults, and produced significant amounts of hanging wall subsidence and footwall uplift. The subsidence and astratal hanging wall tilt extended 15-20 km away from the fault, with up to 6 m of vertical displacement adjacent to the surface rupture, accounting for approximately 85% of the vertical deformation accompanying each of these earthquakes.

Observations of the deformation accompanying these normal faulting earthquakes combined with results of paleoseismological studies led several workers [e.g., *Schwartz and Coppersmith,* 1984; *Machette et al.,* 1991] to propose that

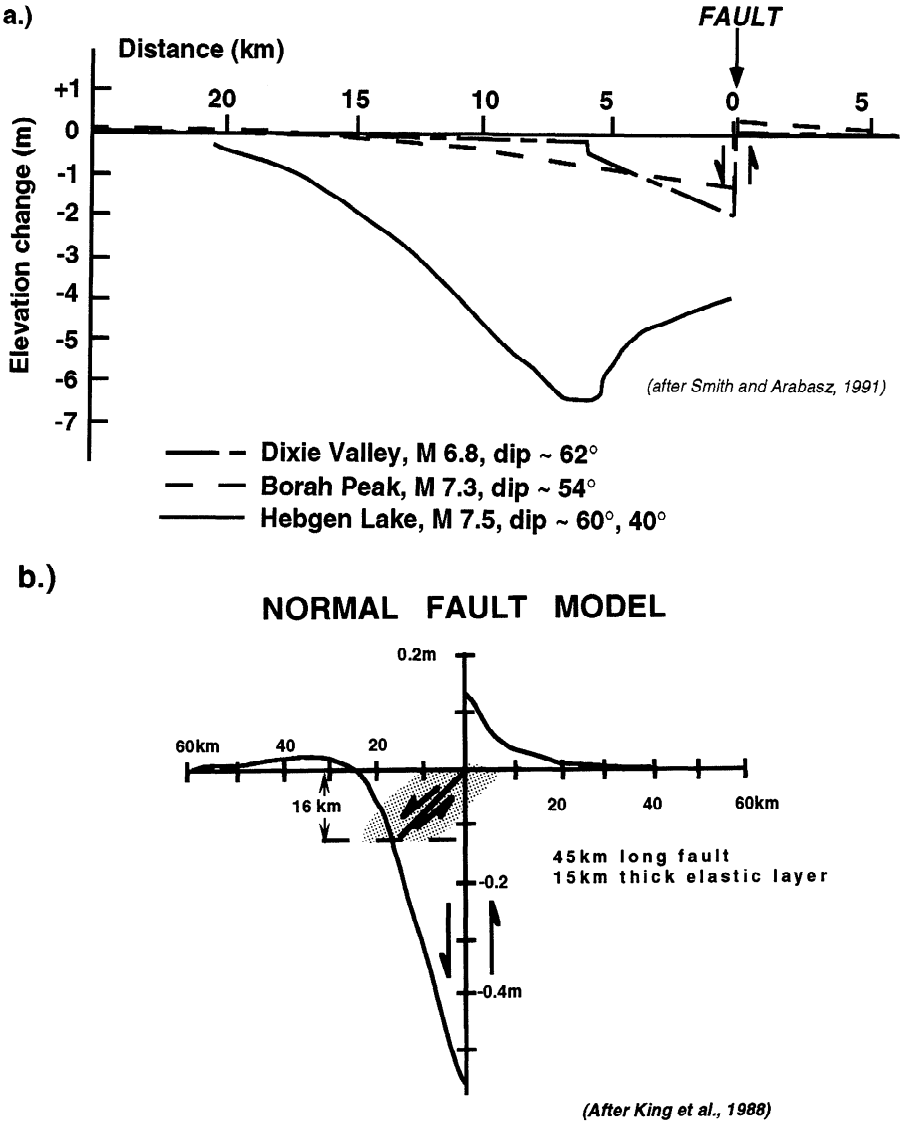

Figure 4. (a) Coseismic and postseismic deformation accompanying large, scarp-forming normal-faulting earthquakes of the Basin and Range , including the M_S = 6.8, 1954 Dixie Valley, Nevada; the M_S = 7.5, 1959 Hebgen Lake, Montana; and the M_S = 7.3, 1983 Borah Peak, Idaho earthquakes; and (b) theoretical surface deformation profile produced by 1 m of normal displacement distributed from 0 to 16 km, on a 45° dipping normal fault [*from King et al.*, 1988].

superposition of multiple, scarp-forming earthquakes on a range-bounding normal fault are reflected by changes in the footwall and hanging wall topography. As a result, variations in topography along strike are cited as evidence supporting variations in the uplift history of a fault and the existence of individual fault segment boundaries.

The similar deformation patterns and seismological characteristics of these three well-studied historic earthquakes led to development of a conceptual working model for normal-faulting earthquakes [*King et al.*, 1988; *Smith and Arabasz*, 1991]. This model allows us to examine the possible occurrence and effects of prehistoric earthquakes on the Teton fault by comparing theoretical deformation profiles with the topographic expression of Jackson Hole and the Teton Range.

Teton Fault

Footwall topography. The overall topography of the Teton Range is dominated by the westward tilt of the range and the symmetrical northward and southward decrease in elevation of the range crest away from a central group of high peaks, including the 4197-m Grand Teton (Plate 1 and Figures 1 and 3). *Fryxell* [1930] noted the Teton range crest is approximately 4 km east of the drainage divide (Plate 1) and suggested that this was due to rapid uplift on an active normal fault (the Teton fault) at the base of the eastern range front. Comparison of the variations in range crest elevation with south to north variations in Quaternary surface offset (Figure 3) and changes in geometry of the Teton fault suggest that the Teton range crest topography may reflect postglacial displacement patterns [*Susong et al.*, 1987; *Smith et al.*, 1990, 1993a]. In contrast, several workers maintain that the relatively high elevation of the high peaks in the Cathedral Group is a product of reverse displacement on the east dipping, Laramide age Buck Mountain fault (Plate 2), the resistance to erosion of the Precambrian igneous and metamorphic rocks that make up the peaks, and uplift and doming of the entire

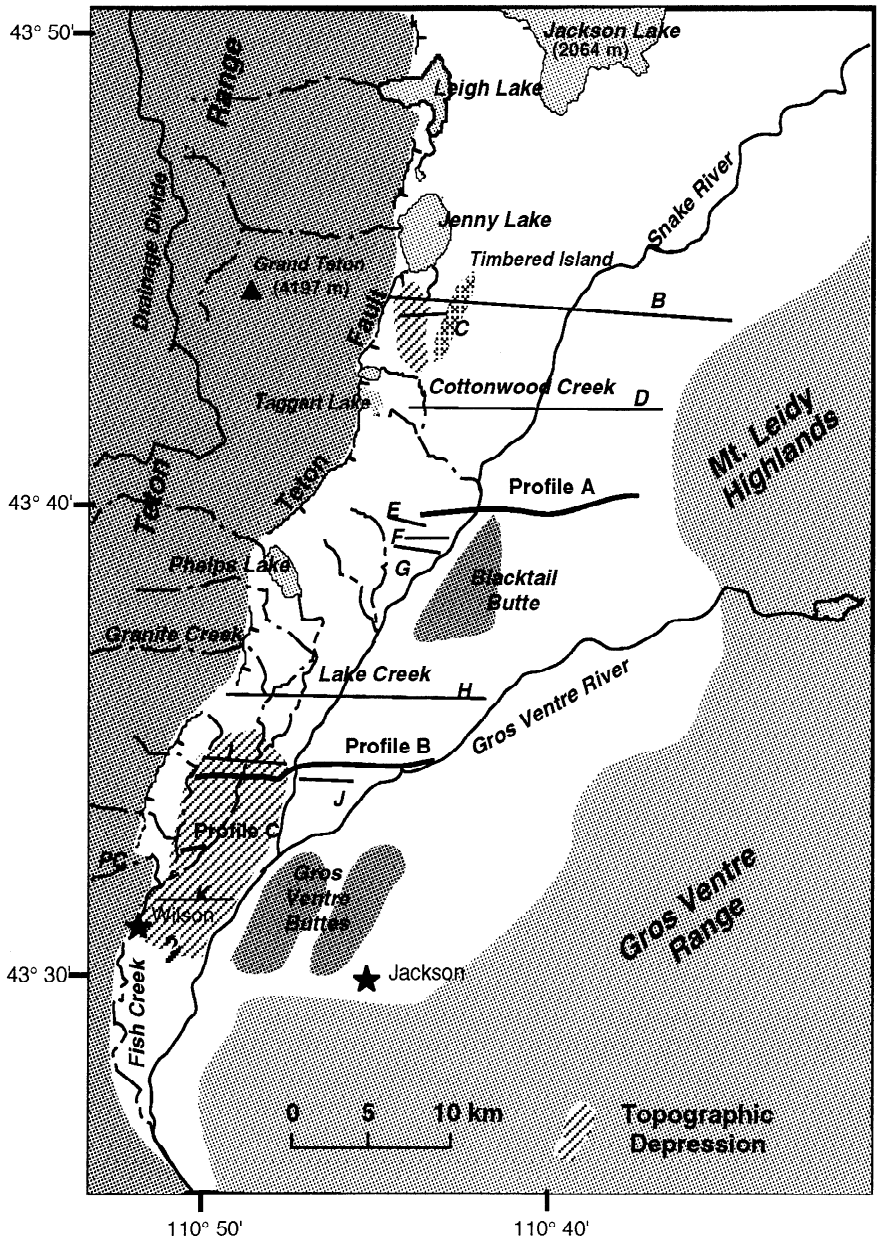

Figure 5. Drainage patterns and location of measured topographic profiles across the central and southern parts of Jackson Hole. PC, Phillips Canyon. B-K indicates locations of *Love and de la Montagne's* [1956] altimeter profiles. Profiles A, B, and C were surveyed as part of this study.

range during the Laramide orogeny [e.g., *Horberg et al.*, 1955; *Love et al.*, 1973; *Smith*, 1991; *Roberts and Burbank*, 1993].

The drainage divide of the Teton Range is in the footwall of several Laramide structures (Plate 2) suggesting that its topographic signature may not be as strongly influenced by Laramide uplift as that of the range crest. The drainage divide generally coincides with the headwalls of Pleistocene glacial cirques and is characterized by a distribution of rock types similar to that found along the range crest (Figure 3). Comparison of the drainage divide topographic patterns with variations in postglacial displacement shows that little or no correlation exists between the two (Figure 3). This may be due to decreased footwall uplift with increasing distance from the bounding normal fault [e.g., *King et al.*, 1988; *King and Ellis*, 1990] so that variations in postglacial displacement along the Teton fault trace have not propagated into the footwall in the past 17,000 years. In addition, postglacial erosion of the drainage divide may have removed any topographic signal caused by faulting. One can not easily discount the dominance of any one or possible contribution of a number of these factors to the topography of the Teton Range. This suggests that variations in footwall topography should be used with care when interpreting uplift across the Teton fault.

Hanging wall topography. In contrast to the apparently negligible impact of postglacial displacements on the footwall topography, the topographic expression of the hanging wall of the Teton fault appears to reflect the influence of a long record of prehistoric earthquakes. Topographic profiles across the floor of Jackson Hole and the anomalous drainage pattern reflecting stream capture on the west side of the valley indicate westward tilt of the valley floor toward the Teton fault (Figures 5 and 6). This topography closely

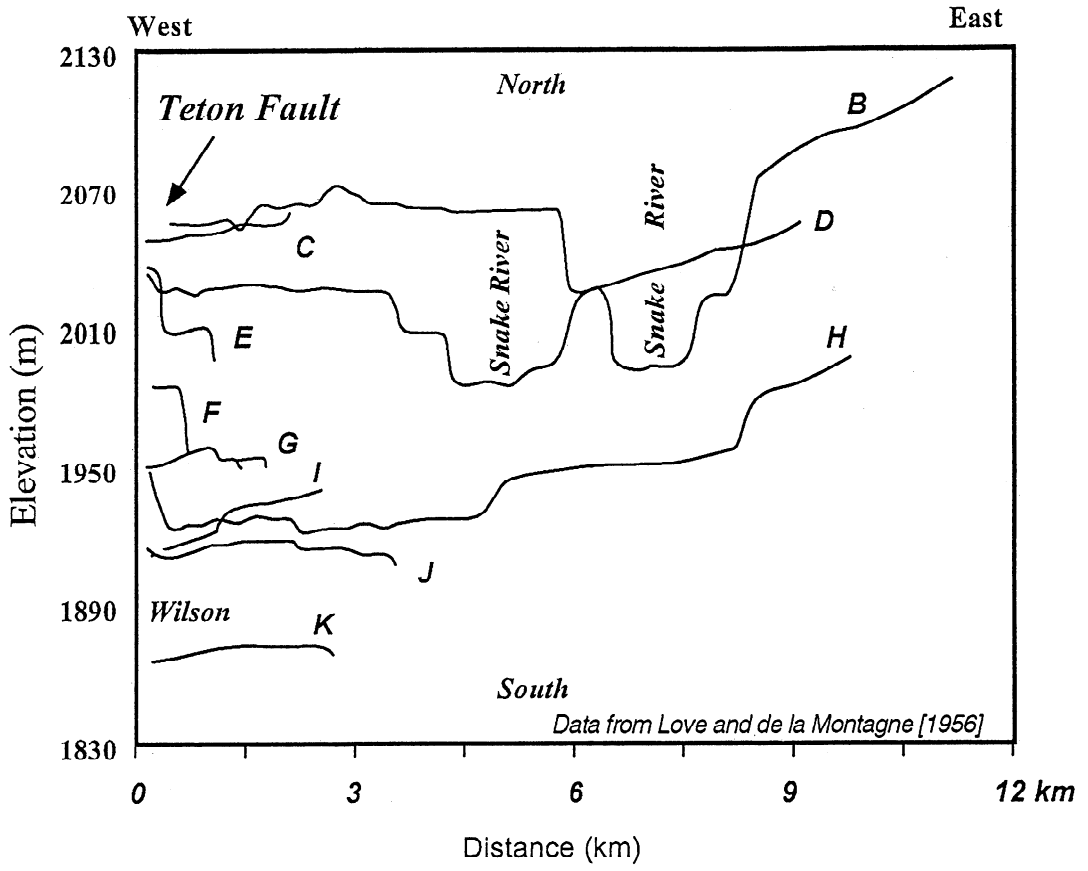

Figure 6. Topographic profiles from *Love and de la Montagne* [1956]. Elevations were determined by altimeter surveys and digitized from original publication. Locations are shown on Figure 5.

resembles the patterns of the accumulated effects of coseismic and postseismic deformation accompanying the historic normal-faulting earthquakes cited previously (Figure 4).

Two elongate topographic depressions on the west side of Jackson Hole were identified on a series of east-west trending altimeter profiles (Figures 5 and 6) by *Love and de la Montagne* [1956]. The depressions are marked by westward tilt and subsidence of the valley floor adjacent to the mountain front and the Teton fault. The tilted surface of the northern depression (Figure 5) is buried by Pinedale glacial moraines deposited during the latest phase of glaciation in Jackson Hole, 13,400-17,000 years ago [*Pierce and Good,* 1990; *Whitlock,* 1993; *Byrd,* 1994]. The southern depression, extends at least 10 km southward from the Granite Canyon moraine complex to the vicinity of Phillips Canyon at the south end of the Teton Range (Figure 5). *Love and de la Montagne* [1956] noted that Cottonwood Creek and the Snake River are perched on the westward sloping surfaces (Figures 5 and 6), implying stream incision occurred prior to tilting, and suggested (prior to recognition of astratal hanging wall tilt as a characteristic of normal-faulting earthquakes) that the westward tilt was a product of displacement on the Teton fault.

The topographic depressions are also evident in the anomalous drainage pattern of streams flowing out of the Teton Range. Rather than flowing directly into the Snake River, streams flowing eastward from the range between Leigh and Taggart Lakes, and south of Phelps Lake (Figure 5), turn away from the Snake River and flow southward along the west side of the valley. This drainage pattern is dramatically illustrated by streams that traverse the southern depression and flow eastward to within 250 m of the Snake River, before turning away from the river and flowing south and west towards the mountain front. The burial of the northern depression by Pinedale age, 13,400-17,000 years, moraines suggests that the stream pattern and westward tilted surfaces developed prior to the latest phase of Pinedale glaciation and may be contemporaneous with, or older than incision of the outwash channels during the previous stage of glaciation in Jackson Hole, 25,000-75,000 years ago [*Smith et al.,* 1993b].

We surveyed three topographic profiles with a Leitz 2000 Total Station to describe the magnitude of westward valley tilt (Figures 5 and 7 and Table 2). Profiles B and C, across the southern depression, show that Lake Creek and the Snake River are perched 4.9 m and 6.5 m, respectively, above the west side of Jackson Hole on a 0.12°-0.17° westward sloping surface. Profile B shows that the Snake River terraces on the east side of the river are also tilted westward, which is consistent with coseismic tilt of the entire valley floor. Longitudinal profiles of streams that traverse the southern depression indicate the western tilt was superimposed on the north to south stream gradients (Figure 7b and Table 2). In contrast, profile A, near the center of the valley, does not show unequivocal tilt west of the Snake River, and the pronounced western tilt and break in slope on the eastern part of the profile are associated with the contact between two alluvial fan surfaces (Figure 7). However, profile A traverses a portion of Jackson Hole marked by positive topographic features, e.g., glacial moraines, Blacktail Butte, and a large alluvial fan, that quite probably obscure any

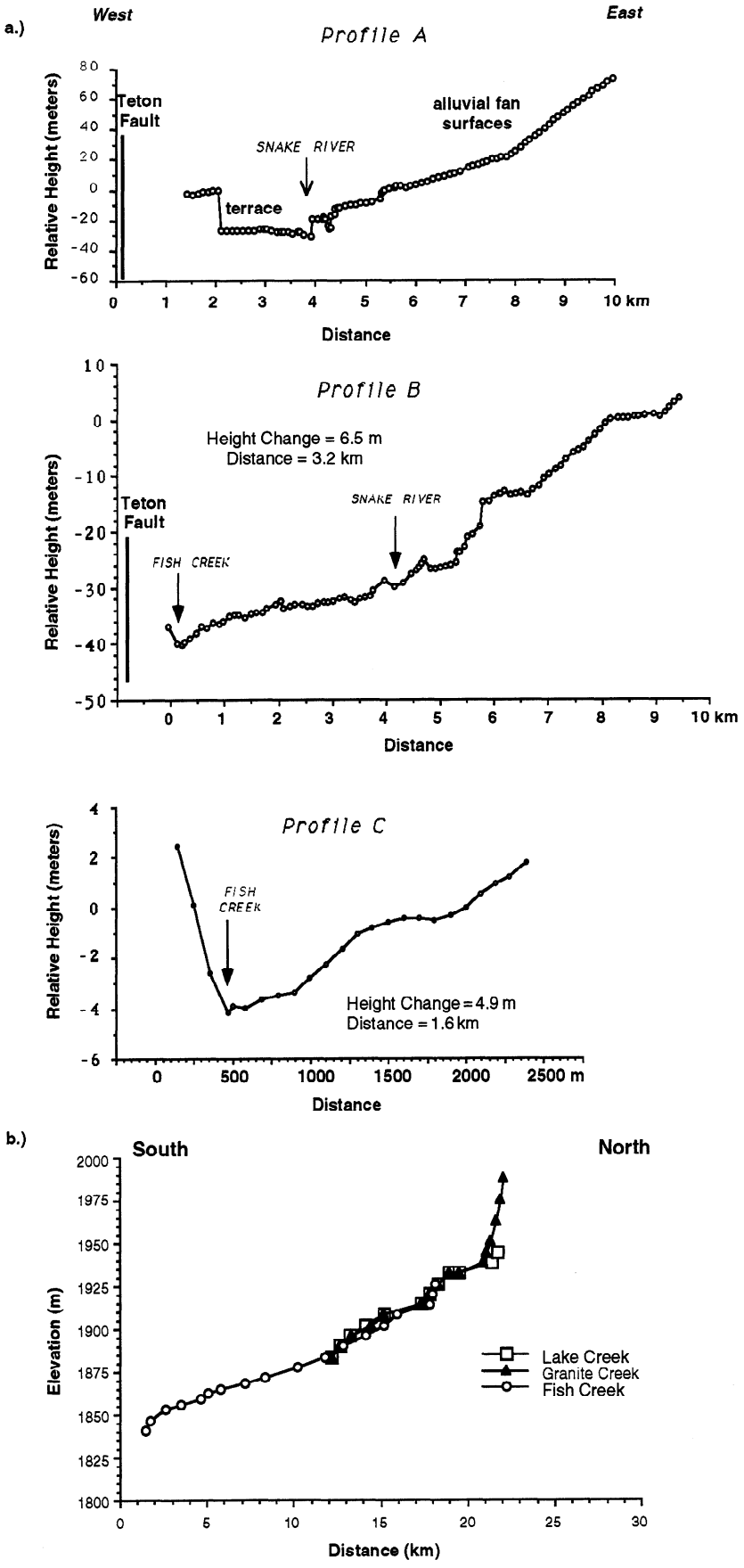

Figure 7. (a) Detailed topographic profiles A, B, and C surveyed as part of this study. Profile locations are shown on Figure 5. (b) Longitudinal topographic profiles of Lake, Granite, and Fish Creeks.

Table 2. Topographic Profile Characteristics

Topographic Profile	Width, km	Height Change, m	Westward Tilt, deg
Profile A			none evident
Profile B			
Snake River (west bank) to Fish Creek	3.2	6.5	0.12
Snake River lower east terrace to Fish Creek	4.8	12.6	0.15
Profile C	1.6	4.9	0.17
Longitudinal Creek Profiles	**Length km**	**Height Change, m**	**Gradient m km^{-1} (Slope, deg)**
Lake Creek	9.0	49	5.4 (0.3)
Granite Creek	8.7	55	6.3 (0.4)
Fish Creek	16.7	85	5.1 (0.3)

See Figure 5 for profile locations

component of western tilt. In addition, the profile crosses the inter basin gravity high (Figure 10) which suggests that less total, and possibly less postglacial, displacement on the Teton fault in this area resulting in less westward tilt of the valley floor.

Models of Hanging Wall Topography

Postseismic and coseismic ground deformation and the overall topographic expression of normal faulting were modeled analytically by *King et al.* [1988], *King and Ellis* [1990], and *Ellis and King* [1991]. Their models show that the theoretical ratio of hanging wall subsidence to footwall uplift is about 4:1 and is remarkably similar to that observed with large historic normal-faulting earthquakes (Figure 4). On the basis of the similarity of between the topographic profiles and the observed and theoretical coseismic deformation profiles we tested a series of forward models to evaluate the subsurface geometry and displacement on the Teton fault.

Our boundary element models used the displacement discontinuity method [*Crouch and Starfield,* 1983] and followed the procedures of *King and Ellis* [1990]. The models invoke a stress-free, brittle, elastic layer, region 1, overlying an inviscid fluid plastic layer, region 2. Region 1 is defined by two horizontal surfaces corresponding to a horizontal datum at the Earth's surface, $\underline{x}_1$=0 km, and a discrete lower boundary, $\underline{x}_1$=12, 15, 18, or 20 km, representing the brittle-plastic transition (Figure 8). This elastic-layer is tethered so that the horizontal displacement, $\underline{u}_3$, and shear stress, σ_{13}, are set to zero along the vertical interface at $\underline{x}_3$ = -100 km. Across the vertical boundary at $\underline{x}_3$ = 100 km the shear and normal stresses, σ_{13} and σ_{33}, are set to zero. The block length is such that the boundary conditions at the edges of the elastic layer do not affect the deformation imposed by faulting in the central portion of the block at x_3 = 0 km (Figure 8).

A series of forward models was tested in which we varied the fault geometry, the amount and depth distribution of displacement on the fault, the thickness of the elastic layer, and the elastic constants in the plastic layer to evaluate the resulting surface displacements. Selection of the model parameters was aided by the results of our models of aseismic height changes observed across a 1st order leveling line across the Teton fault (J.O.D. Byrd et al., Geodetic evidence for aseismic deformation across the Teton fault, Wyoming, submitted to *Journal of Geophysical Research,* 1994). The resulting vertical surface displacements were compared to the detailed topographic profiles to evaluate the applicability of the model geometry and displacements.

The boundary element model results suggest that the westward tilt (observed on profile B) is consistent with 110 to 125 m of dip-slip displacement on the Teton fault, over a depth range of 0 to 15 km and dips of 45° to 75°E (Figure 8). The 60° and 75°E dipping fault models predict cumulative footwall uplift of 6-16 m. The 45°E model predicts that footwall uplift occurs more than 2 km into the footwall. Comparable surface offsets of 11-17 m have been measured in glacial deposits along this part of the Teton fault (Figure 3).

Net tectonic offsets of 2.8 and 1.3 m, associated with two prehistoric surface ruptures at 8040-7740 years and 7190-6880 to 4870-4815 years, were exposed in a trench across the Teton fault observed, 5 km north of Profile B [*Byrd,* 1991; *Byrd,* 1994]. These displacements are comparable to those observed following the 1983 Borah Peak earthquake [*Crone and Machette,* 1984] and other M=7.0 ± 0.3 events [e.g., *Bonilla et al.,* 1984]. Fault dislocation models of coseismic slip accompanying the 1959 Hebgen Lake and 1983 Borah Peak earthquakes [*Barrientos et al.,* 1987] suggested that the surface displacements accompanying these earthquakes could be approximated by 7-11 m, and 1.4-2.2 m of slip on one or two planar normal faults, respectively.

Comparison of the above observations and model results with our modeling of the Teton fault suggest that the postglacial history of the Teton fault may be characterized by coseismic displacements similar to those that accompanied the 1983 Borah Peak earthquake. Recognizing that the 110-125 m of modeled displacement are minimum values since they do not incorporate postseismic slip, the displacements may reflect about 50 Borah Peak events on the Teton fault in the past 25,000-75,000 years. This corresponds to a recurrence interval of 360-1,450 years based on the apparent lack of surface rupturing events on the Teton fault in the past 4850-7000 years [*Byrd,* 1991; *Byrd,* 1994]. If, however, the tectonic displacements measured in the trench represent minimum values, the 7-11 m of modeled Hebgen Lake slip may be more applicable, in which case 10 to 16 M 7+ postglacial earthquakes may have ruptured the Teton fault. This upper limit of slip per earthquake corresponds to a 1130-7020 year recurrence interval. In both instances, the predicted recurrence intervals are of the same order as predicted from contemporary seismicity of the Teton-Jackson Hole-Gros Ventre area [*Doser and Smith,* 1983; *Gilbert et al.,* 1983] and paleoseismological studies of the Teton fault [*Byrd* , 1994].

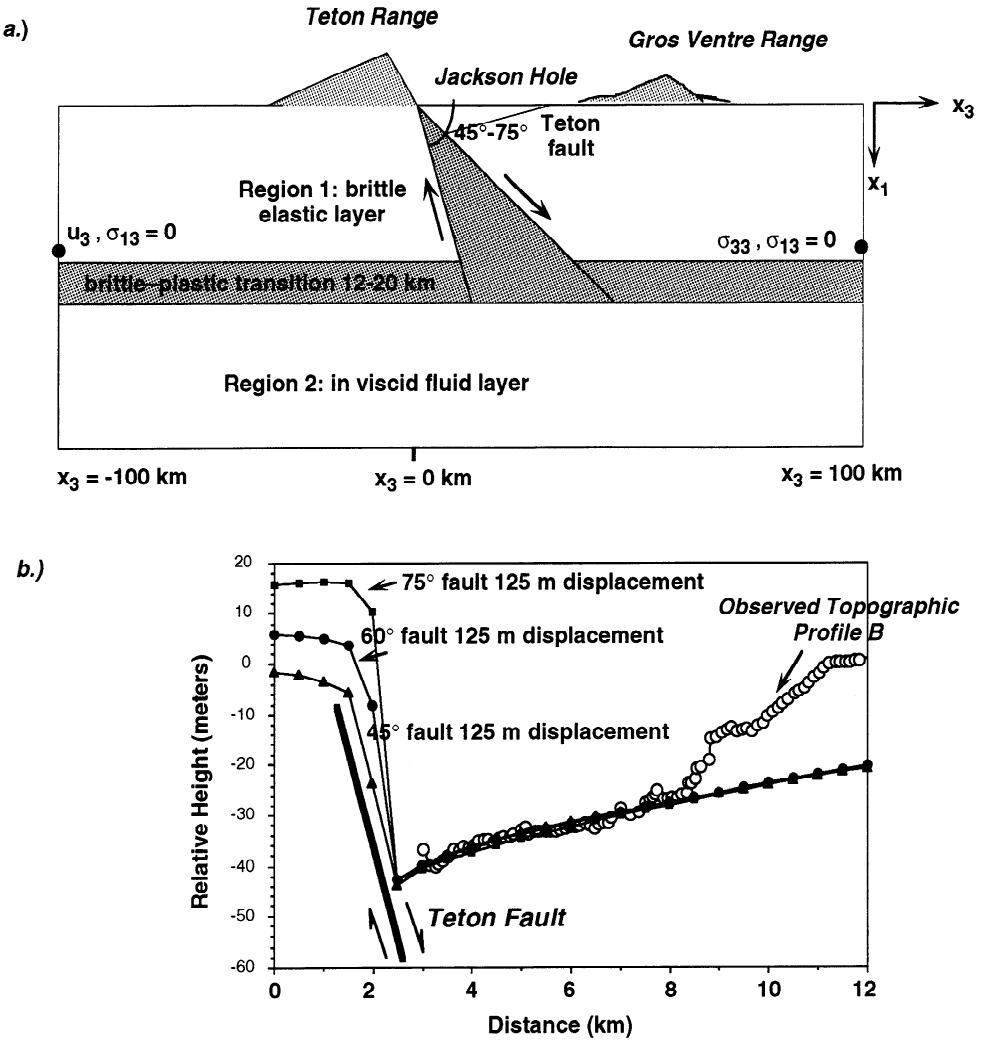

Figure 8. (a) Boundary element model configuration for fault dislocations used in this study; and (b) Surface deformation produced by boundary element models. Magnitude of displacement, depth range of displacement, and fault dip for each profile are shown.

Subsurface Geometry of the Teton Fault

We collected detailed gravity data along four hanging wall profiles and combined that with existing seismic refraction and gravity data [*Behrendt et al.*, 1968] in the Teton-Jackson Hole area to assess the subsurface geometry of the Teton fault.

Seismic Refraction Profile

Seismic refraction data were collected along an east-west trending 27-km-long profile across the floor of Jackson Hole (Plate 2) in 1964 by *Behrendt et al.* [1968] and *Tibbets et al.* [1969]. Shallow dynamite charges were exploded at three shot points, and the data were recorded by a series of eight linear geophone arrays, with individual geophone spacing of 500 m. Geophone locations were accurate to 50 m to 100 m, and an error of ± 0.01 s was ascribed to the hand-picked arrival times [*Tibbetts et al.*, 1969].

Using standard forward modeling and delay time analysis techniques, *Behrendt et al.* [1968] and *Tibbetts et al.* [1969] estimated a throw of 7 km across the Teton fault. They identified two prominent impedance contrasts and a three-layered velocity structure beneath Jackson Hole (Table 3 and Figure 9). *Behrendt et al.* [1968] viewed the Teton fault as a 35° to 45°E dipping structure, or possibly as a series of steeply dipping down-to-the-east normal faults at the west end of the profile. In contrast, *Tibbetts et al.* [1969] maintained the poor data quality along the west part of the profile precluded determination of the geometry of the Teton fault. Both groups of authors noted that their interpretations were hampered by poor definition of the location of the Teton fault trace relative to the west end of the refraction profile. We also note that the lack of ray path coverage west of the fault precluded direct imaging of the fault.

Inverse ray-tracing models. We tested a series of two-dimensional inverse, ray-tracing models of the U.S. Geological Survey (USGS) refraction data to evaluate the subsurface geometry of the Teton fault and Jackson Hole. Unfortunately, the original data records and tables of travel times and distances along the profile were lost, so travel times and horizontal locations were digitized from the original drafted plots provided by J. Behrendt (USGS, personal communication, 1989). The digitization introduced additional errors to the travel time and distance data, and standard errors ± 0.02 s and ± 75 m were incorporated into the inverse modeling.

We performed multiple iterations of the ray-tracing

Table 3. Seismic Refraction Model Parameters

Shot Point	Layer 1 Velocity, km s^{-1}	Layer 1 Thickness, km	Layer 2 Velocity km s^{-1}	Layer 3 Velocity km s^{-1}
	Behrendt et al. [1968]			
(2a)	2.45[1]		3.8	6.8
(2b)	2.45	1.4	4.2	6.1
(2c)	2.45		4.1	6.7
	Tibbetts et al. [1969]			
(2a)	2.4	0.5	4.0	6.7
(2b$_W$)	2.2	0.7	3.4	5.7
(2b$_E$)	2.5	0.7	4.1	6.8
(2c)	2.4	0.3	3.8	5.7
	This Study			
30° E fault	2.10	1.0	4.24	6.10
45° E fault	2.23	0.4	4.14	6.08
60° E fault	2.09	0.3	4.48	6.16
75° E fault	2.20	0.8	4.52	6.14

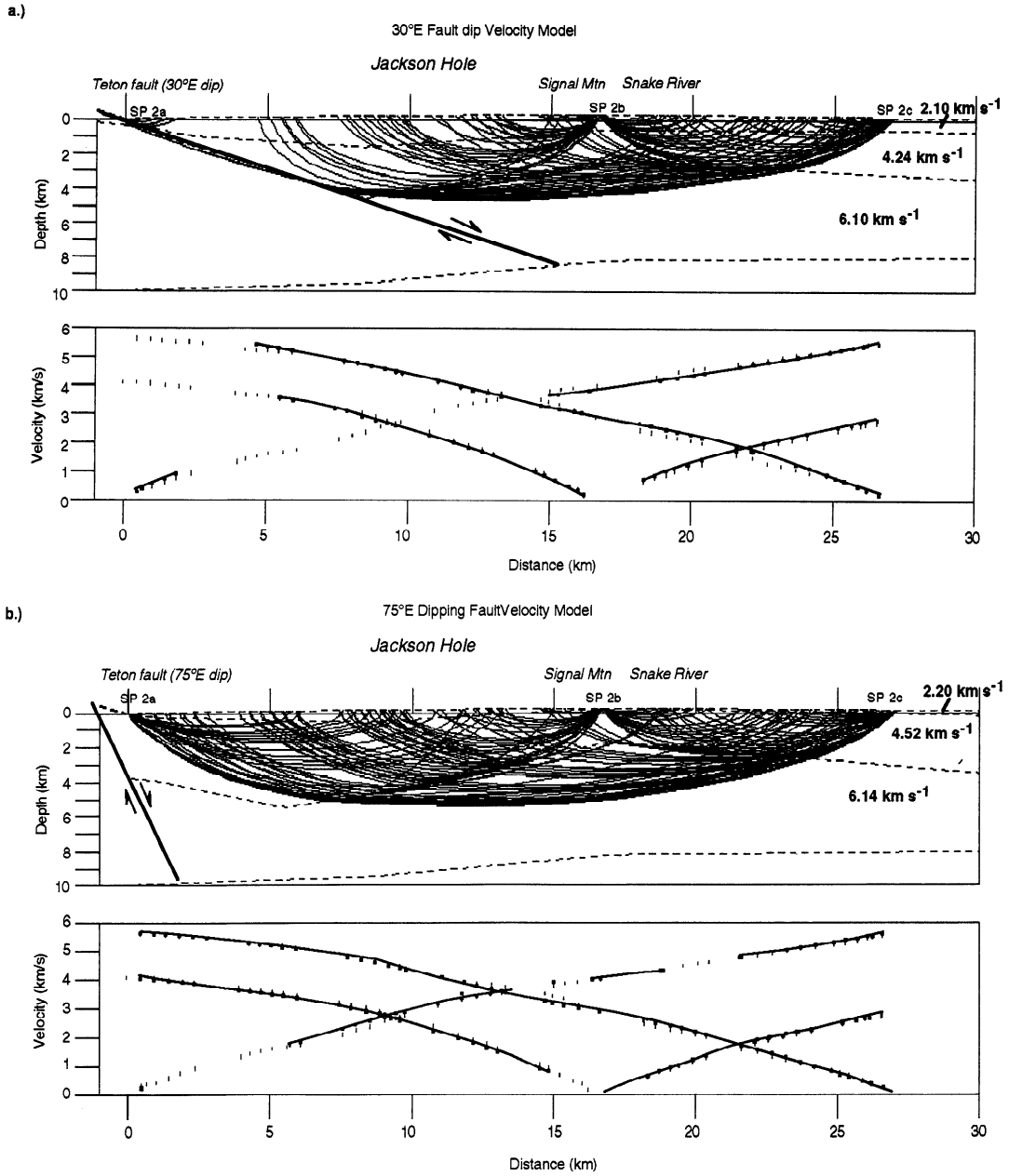

Figure 9. Results of ray-tracing models of seismic refraction data depicting (a) 30°E and (b) 75°E dipping Teton fault. Labels indicate average *P* wave velocities for each layer.

Table 4. Seismic Refraction Model Results

Velocity Model	χ^2	RMS Travel Time Residual	Number of Travel Time Points Modeled
No fault (4 layer)	1.443	0.060	96
No fault (3 layer)	2.195	0.074	103
30°E Dipping fault	18.043	0.211	122
45°E Dipping fault	11.209	0.167	112
60°E Dipping fault	4.942	0.111	133
75°E Dipping fault	3.516	0.093	131

inversion (Table 4) using the methodology of *Zelt and Smith* [1992]. Convergence of each iteration to the digitized data was evaluated by comparing the model resolution, the χ^2 parameter, RMS travel time residual, and the velocity structure of each iteration. Three to six iterations generally produced a best fitting model that resolved the digitized data with relatively small RMS values. However, if the best fit model incorporated an unrealistic velocity structure, we adjusted the model parameters and ran additional inversions based on our general knowledge of the regional stratigraphy.

Our ray-tracing modeling results suggest that the Teton fault dips from 60° to 90°E (Figure 9 and Table 4), and that lateral velocity variations of up to 0.25 km s^{-1} characterize the hanging wall velocity structure across the entire length of the profile. (The constant lateral-velocity structure and shallow dip ascribed to the Teton fault by the *Behrendt et al.* [1968] and *Tibbetts et al.* [1969] models' showed a poor-fit to the digitized data using our methodology.) It should be noted, however, that no seismic rays crossed the Teton fault itself in any of the models (Figure 9), and the smaller χ^2 and RMS values of the

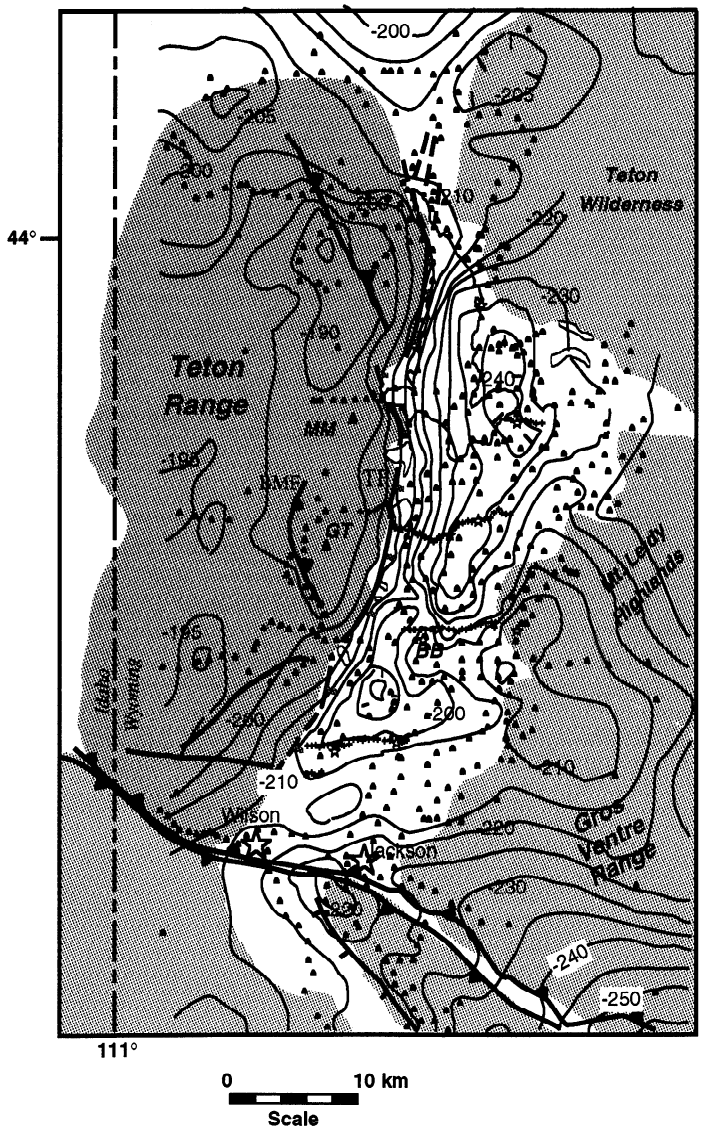

Figure 10. Complete Bouguer anomaly map for the Teton-Jackson Hole area. Contour interval is 10 mGal. Station locations are indicated by small triangles.

best fit steeply dipping or "no fault" models (Table 4) are a product of the deeper penetration of rays from shot point 2a rather than direct imaging of the fault. As a result, the inverse ray-tracing model results produce an equivocal interpretation of the Teton fault geometry.

In contrast to the equivocal results at the west end of the profile, the ray-tracing models resolved the geometry of the intermediate and deep refractors quite well along the central and eastern parts of the profile (Figure 9). The rays did not resolve the shallow refractor, however, which is interpreted as being near the base of the Tertiary to Quaternary basinal deposits, so that the depth of the hanging wall basin is poorly determined by the ray-tracing models.

Gravity Models

We collected gravity data, observed accuracy of approximately 0.1 mGal (with a Worden Geodesist gravimeter at 300-m to 500-m intervals), along four east-west trending gravity profiles across the floor of Jackson Hole (Plate 2). Station locations and elevations were surveyed with a Leitz 2000 Total Station, resulting in ± 0.01 m of elevation control at each station, and daily drift corrections were established by reoccupying local base stations at maximum intervals of 3 hours. A complete Bouguer corrected anomaly (Bouguer density 2670 kg m^{-3}) was calculated for each station by V. Bankey (USGS). A local complete Bouguer anomaly map (Figure 10) was produced by supplementing the reduced detailed data with reconnaissance gravity data collected by *Lavin* [1957] and *Behrendt et al.* [1968].

Lavin [1957] noted that Jackson Hole is characterized by two distinct gravity lows and a 6 mGal km^{-1} gradient along the east side of the Teton Range. He developed a series of forward gravity models of the Teton-Jackson Hole region (Figure 11a) that suggested the Teton fault dips 60° to 90°E and has a maximum total throw of approximately 5.5 km. *Lavin and Bonini* [1957] suggested the relatively broad gravity gradient associated with the northern Teton fault (Figure 10) implied a "step-fault" geometry, where the major displacement was located on a 60°E dipping fault 3 km east of the range front

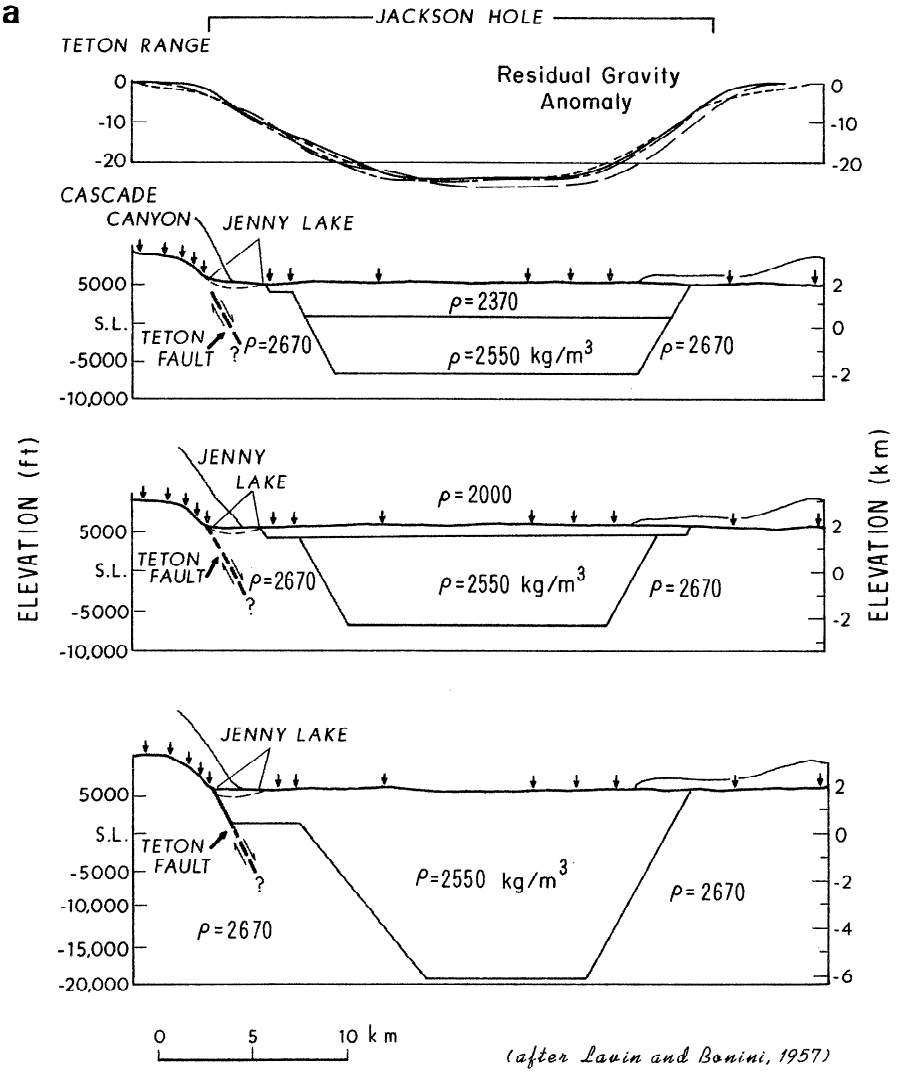

Figure 11. Density and velocity models of the hanging wall of the Teton fault, Jackson Hole. (a) Forward gravity modeling results of *Lavin and Bonini* [1957] and (b) Gravity and seismic refraction interpretation of *Behrendt et al.* [1968].

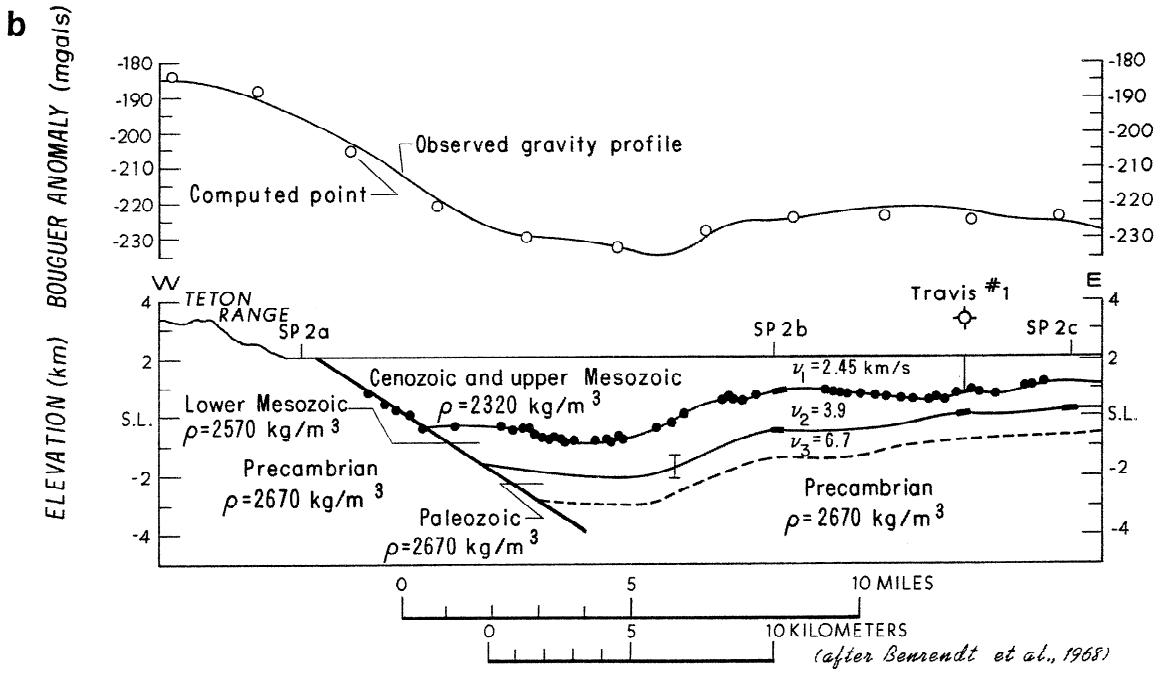

Figure 11. (continued)

(Figure 11a). *Behrendt et al.* [1968] maintained the gravity gradient also supported a 35° to 45°E dip for the Teton fault (Figure 11b).

We developed a series of two-dimensional forward gravity models of our detailed data to better determine the subsurface Teton fault geometry (Figure 12). The number, geometry, and density of individual layers were adjusted from those suggested by *Lavin* [1957] and *Behrendt et al.* [1968] and the results of the ray-tracing models. Constant layer density contrasts were maintained, and a 3-5 mGal/km regional gradient was removed from each gravity profile. The goodness of fit of each forward model was based on of resolution the observed data and each model's L_2 norm.

Hanging wall geometry of the Teton fault. The gravity data show that Jackson Hole is underlain by two distinct sedimentary basins, associated with -240 mGal and -220 mGal gravity lows, separated by a pronounced WNW trending gravity high (Figure 10). The basins are filled with 2350 kg m^{-3} density rocks that include Miocene volcaniclastic and lacustrine strata, the ~2.0 Ma Huckleberry Ridge Tuff, and Quaternary glacial deposits. Basin depths vary from west to east from 0.5 to 1.5 km next to the Teton fault to 2 to 2.5 km over the centers of the basins and 1 km on the west side of Blacktail Butte (Figure 12). Mesozoic(?) sedimentary rocks, 2500 kg m^{-3} density, are inferred to underlie the eastern and central parts of the basins (Figure 12). Although up to 5 km of Mesozoic rocks are exposed east of Jackson Hole [e.g., *Behrendt et al.*, 1968], these units are absent in the central and southern parts of the Teton Range suggesting they do not extend across the basin. The gravity models (Figure 12) suggest that 2600 to 2800 kg m^{-3} density, crystalline and Paleozoic(?) rocks are present at shallow depths below the western side of the basin against the Teton fault.

The interbasin gravity high (Figure 10) may represent an area of relatively shallow basement rocks that may correspond to a decrease in throw across the Teton fault. This inferred displacement gradient, and its coincidence with a 25° change in strike of the Teton fault in this area, has been interpreted as a fault segment boundary [*Susong et al.*, 1987; *Smith et al.*, 1990, 1993a]. *Ostenaa* [1988] discounted the existence of a segment boundary, and results of our subsequent paleoseismological studies [*Byrd*, 1994] suggest that this area of the Teton fault may correspond to a conservative barrier to rupture propagation [*King and Nabelek*, 1985; *King*, 1986]. The interbasin high may also reflect inherited Laramide-age structural relief feature, based on its general coincidence with the westward projection of the regional WNW trending gravity anomaly related to the Gros Ventre Range (Figure 10).

Footwall geometry of the Teton fault. The gravity models require the presence of relatively high density rocks, 2800 kg m^{-3}, in the footwall of the Teton fault to approximate the relative gravity high associated with the Teton Range (Figures 10 and 12). Amphibolite, diabase dikes, and banded gneiss crop out within the range [*Reed and Zartman*, 1973], and it is possible that a relic mafic body that fed the 1.7 Ga diabase dikes is the source of this -195 mGal gravity anomaly. In addition, the positive gravity anomaly generally coincides with the hanging wall block of the Buck Mountain fault within the Teton Range [*Smith*, 1991]. Reverse displacement on this Laramide structure may have placed relatively high density rocks over the lower density 2.5 Ga Mount Owen Quartz Monzonite [*Reed and Zartman*, 1973] producing the -195 mGal elongate gravity anomaly characteristic of the range in this area (Figures 10 and 12).

Geometry of the Teton fault. The pronounced 3 to 6 mGal/km gravity gradient and the convex-upward anomaly that mark the west side of Jackson Hole suggest that high, 2800 kg m^{-3}, density rocks within the Teton Range have either been displaced by and abut the Teton fault, or that the fault is a shallow, 30°E, dipping structure (Figures 10 and 12). Previous suggestions that the gravity anomaly represents a 2-5 km wide fault zone [*Lavin and Bonini*, 1957; *Behrendt et al.* 1968; *Tibbetts et al.*, 1969] have been discounted by detailed mapping along the entire mountain front [*Gilbert et al.*, 1983;

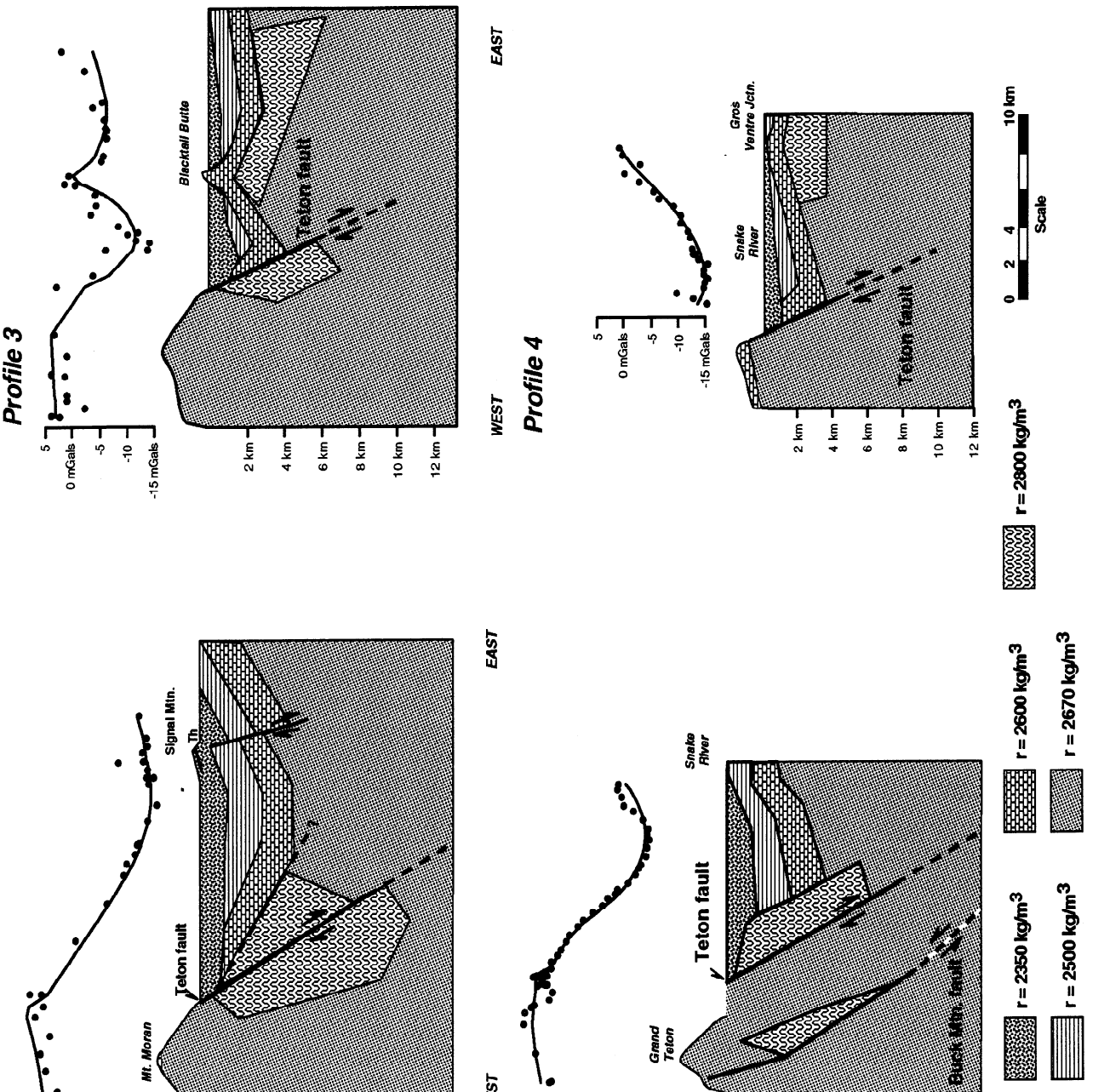

Figure 12. Gravity modeling results of profiles 1-4 for this study (locations are shown on Figure 3).

Susong et al., 1987; *Smith et al.*, 1993a] and seismic reflection and refraction profiling across Jackson Lake [*Smith et al.*, 1993b].

The gravity model results also suggest 2800 kg m^{-3} density rocks abut the Teton fault in the central and northern parts of the range, effectively masking the expected gravity signature associated with a normal fault. We believe this apparently elongate high density body may be associated with Laramide or older structures that have been offset or inherited by the Teton fault. For example, the Forellen and Buck Mountain fault zones within the Teton Range and northwest striking structures that crop out at Blacktail Butte and in the Gros Ventre Range to the southeast (Plate 1 and Figure 2) coincide with the relative gravity high. Alternatively, the high-density rocks may represent the buried source areas of the volcanic rocks of the Miocene Colter Formation as proposed by *Barnosky* [1984].

In the southern part of Jackson Hole, the gravity models suggest that the Teton fault is a single 30° to 70°E dipping structure that has juxtaposed 2670 kg m^{-3} footwall rocks against 2600 kg m^{-3} rocks in the hanging wall (Figure 12). The apparent absence of 2800 kg m^{-3} rocks adjacent to the Teton fault coincides with the southern termination of the NNW striking Buck Mountain fault and the overall absence of Laramide reverse faults in the southern portion of the Teton Range (Plate 2).

Our gravity models suggest throw on the Teton fault ranges from 2.5 to 8 km based on a variety of assumptions regarding the pre-extension configuration of the Teton Range, the interpreted range of depths of the 2600 to 2800 kg m^{-3} rocks, and the apparent 0.5-1.5 km thickness of Tertiary-Quaternary, 2350 kg m^{-3} deposits adjacent to Teton fault. If the approximately 2 km of topographic relief across the Teton range front in the vicinity of Mount Moran are entirely a product of displacement on the Teton fault, then addition of the thickness of Tertiary-Quaternary yields a total throw of 2.5-3.5 km. This estimated throw is also indicated if the Paleozoic-Precambrian contact was continuous across the Teton range front in this area prior to the initiation of extension (Figure 12). A maximum 8 km of throw is also consistent with the maximum depths of 2600 to 2800 kg m^{-3} rocks predicted by the gravity models (Figure 12). This estimate is consistent with that of previous workers (Table 1), studies of Laramide structures within the Teton Range [e.g., *Horberg et al.*, 1955; *Edmund*, 1951; *Smith*, 1991], and results of fission track analyses [*Roberts and Burbank*, 1993] that indicate faulting and uplift of the Paleozoic and older rocks occurred prior to initiation of extension.

The generally limited control on the nature and extent of pre-extensional deformation of the Paleozoic-Precambrian contact, and the inherent ambiguity of the gravity and seismic refraction models limit the reliability of maximum throw estimates. By contrast, the relatively limited range of estimated thicknesses of Quaternary-Tertiary rocks from the gravity models and the independent estimates of 2.5 to 3.5 km of throw by several different methods, suggest that this is a more likely estimate of throw across the Teton fault.

Paleomagnetic Evidence for Quaternary Deformation on the Teton Fault

To evaluate the magnitude of Quaternary tilt across the Teton fault, we collected and analyzed paleomagnetic data from 68 sites in the ~2.0 Ma Huckleberry Ridge Tuff in the footwall and hanging wall of the Teton fault (Plate 2). We compared our paleomagnetic data from the Teton area (Table 5 and Figure 13) with the Huckleberry Ridge Tuff reference direction determined from *Reynolds'* [1977] extensive study of late Pliocene and Quaternary volcanic rocks of the Yellowstone Plateau. We assume that Reynolds' ensemble of Huckleberry Ridge Tuff data has averaged out any local, nonsystematic deformation and is thus a reliable "reference" data set for the tuff. *Anders et al.* [1989] made a similar comparison in their study of a normal fault bounded valley, approximately 30 km southwest of the Teton Range, and concluded the apparent tilt of the Huckleberry Ridge Tuff was a product of emplacement on preexisting topography.

The Huckleberry Ridge Tuff is a compound ash flow tuff that erupted from a source area in the southwest portion of the

Table 5. Summary of Previous Paleomagnetic Investigations of Huckleberry Ridge Tuff

Study	Location[a]	N[b]		D[c]	I[c]	α^{95}[d]	k[e]	Comments
		Sites	Samples					
Reynolds [1977]	Yellowstone Park area	4		213.0	-2.9	2.4	40	in situ
			12	214.5	-2.2	3.5	20	in situ
		41		215.5	-0.9	7.1	116.7	in situ
Anders et al. [1989]	Swan Valley, east Idaho	10		206.4	-0.6	3.4	181.0	in situ
	Ririe Reservoir, east Idaho		10	214.0	2.0	3.3	211.7	corrected
Morgan [1992]	Deadman's Bar, Jackson Hole		8	206.1	3.7	4.4	161.2	in situ
	Cliff Lake, west Montana		6	216.3	-3.8	4.6	210.9	corrected

[a] Ririe Reservoir is about 45 km west of Jackson, Wyoming. Cliff Lake is about 90 km northwest of the Teton Range on the west side of the Madison River valley.

[b] Number of independently oriented samples or separate sites studied.

[c] D, declination, and I inclination of the site or study mean direction of magnetization (in degrees clockwise from north and positive downward), in situ coordinates.

[d] Semi-angle, in degrees, of the 95% cone of confidence about the mean direction.

[e] *Fisher's* [1953] best estimate for the precision parameter of a statistical grouping of N vectors.

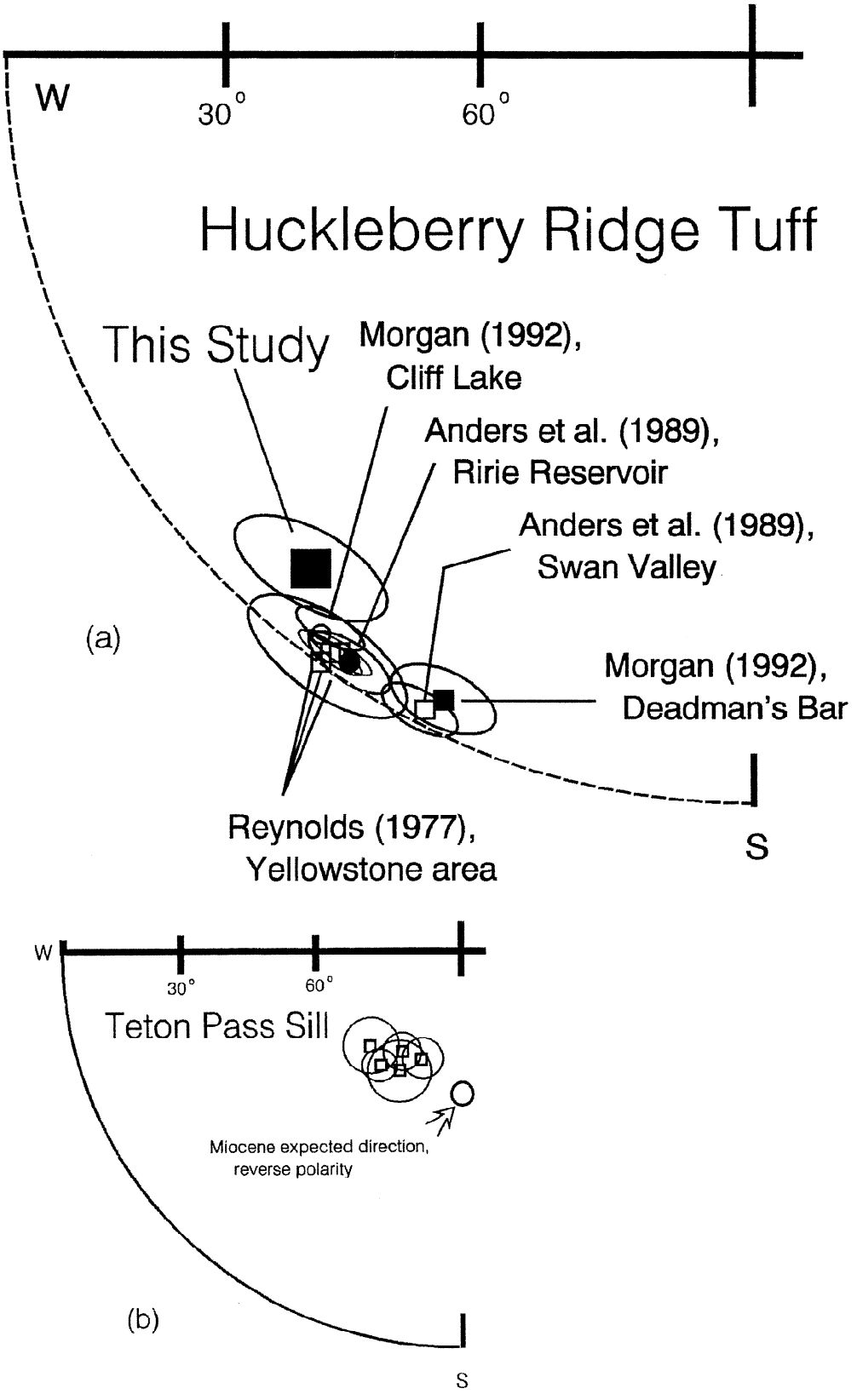

Figure 13. (a) Equal area projection of Huckleberry Ridge Tuff data reported in previous studies (Table 5) and the grand in situ mean obtained in this study. (b) Partial equal-area projection of in situ site mean directions for the five sites in the late Miocene andesite sill southeast of Teton Pass. Also shown are the projected cones of 95% confidence about each mean and the general Miocene expected direction, calculated from the North America Miocene paleomagnetic pole from *Mankinen et al.* [1987]. Open (solid) symbols refer to upper (lower) hemisphere projections. Squares denote in situ data; circles denote data that have been corrected for local tilt; the tilt correction applied is based on the orientation of eutaxitic structures.

Yellowstone Plateau, 10-20 km north of the Teton Range [*Christiansen,* 1982]. It is characterized by a south-southwest declination and very shallow magnetic inclination (Table 5 and Figure 13), which *Reynolds* [1977] considered indicative of eruption during either a high-amplitude "excursion" of the geomagnetic field or a polarity transition. A 2.057 Ma ± 0.008 Ma $^{40}Ar/^{39}Ar$ laser fusion age on sanidine [*Sarna-Wojcicki and Pringle,* 1992] is also consistent with eruption of the ash-flow tuff during either the R-N or N-R transitions associated with the Reunion normal polarity event in the Matuyama chron.

Previous studies of the paleomagnetism of the Huckleberry Ridge Tuff in the Yellowstone region [*Reynolds,* 1977; *Anders et al.,* 1989; *Morgan,* 1992] are summarized briefly in Table 5. *Reynolds* [1977] sampled the widest distribution of the tuff, and we consider his study to be the most robust. *Morgan* [1992] reports data from only two well-defined sites, and *Anders et al.* [1989] obtained data from 11 sites 30-50 km southwest of the Teton-Jackson Hole area.

Methodology

Our sampling strategy was designed to cover as much of the geographic distribution of the ash flow tuff in the footwall and hanging wall of the Teton fault as possible. We also sampled five sites (TP1-5) in an andesite body interpreted to be a 8.1 ± 0.9 Ma (whole rock K-Ar date) sill in Paleozoic strata at the southern end of the Teton Range [*Love et al.,* 1992]. In all cases, independently oriented samples were obtained using a portable field drilling apparatus with nonmagnetic stainless steel drill bits. Specimens were prepared into standard right cylinders in the laboratory.

Instrumentation employed in measurement of the natural remanent magnetization (NRM) and demagnetization is described by *Geissman et al.* [1991]. Interpretation and reduction of individual demagnetization results involved visual inspection of orthogonal demagnetization diagrams and projections of specimen directions. Where a stable endpoint (as defined by the colinearity of several demagnetization points in a trajectory toward the origin) could be recognized a least-squares linear fit [*Kirschvink,* 1980] was obtained for the sequence of data points. Linear segments were never anchored to the origin, and those accepted had maximum angular deviation angles less than 10°. In some cases we combined least squares stable endpoint data with remagnetization circle data to obtain a refined determination of a site mean direction.

Paleomagnetic Data

Data from our study confirm the unusual field direction recorded by the Huckleberry Ridge Tuff (Figure 13a and Table 6). In this contribution, we summarize most of the data from our paleomagnetic investigation and only briefly discuss the relatively complex demagnetization behavior of this ash flow tuff. In a separate contribution (J.W. Geissman et al., manuscript in preparation, 1994) we more thoroughly discuss the paleomagnetism and rock magnetism of the rocks sampled.

At sites where the south-southwest declination and shallow inclination was the principal contributor to the NRM, either alternating field or thermal demagnetization served to adequately define the magnetization in a linear trajectory to the origin (Figures 14f, 14g, and 14h). The characteristic magnetization is of high median destructive induction and moderate to high laboratory unblocking temperatures. Over half of the sites in our collection were characterized by a more complex NRM, with a magnetization of moderate to steep positive inclination, usually north seeking, superimposed on the characteristic magnetization (Figures 14b, and 14e). In some sites, a combination of thermal demagnetization to moderate (about 300 °C) temperatures followed by AF demagnetization served to fully isolate the south-southwest declination, shallow inclination magnetization (Figures 14a, and 14b). In other cases, progressive demagnetization served only to define a great circle, curvilinear trend to individual remanence measurements. Great circles were fit to these data, and where possible we combined both stable endpoint and great circle results to further refine site means (Table 6).

The response to progressive demagnetization by rocks of the Huckleberry Ridge Tuff is complicated for two reasons. (1) At many sites the magnetic mineralogy of relatively poorly welded portions of the tuff is extensively oxidized and secondary components of magnetization comprise well over 75% of the NRM. Resolution of the primary thermoremanent magnetization (TRM) at these sites is difficult, if not impossible. (2) The second reason is more ad hoc, yet nonetheless of equal importance. During geomagnetic field transitions, recent studies show the direction of the magnetic field can change rapidly [*Coe and Prevot,* 1992], suggesting that the remanence in the Huckleberry Ridge tuff may also be complicated by potentially rapid field variations over short time periods during TRM blocking. Overall, for the majority of the sites in our collection, we feel that we have either adequately separated the characteristic magnetization from a positive inclination, normal polarity secondary magnetization or defined the characteristic magnetization by combined stable endpoint and remagnetization circle analyses.

All five sites in the sill at the south end of the Teton Range were collected in a large roadcut, with no obvious structural breaks between any of the sites. The rocks from this intrusion are characterized by straightforward demagnetization behavior, with stable endpoints well-defined over a broad range of peak demagnetizing fields and/or unblocking temperatures (Figures 14i and 14j). At the site level, sample directions are well grouped, the largest α_{95} value being 6.1° (Figure 13b and Table 6). Mean directions from all five sites are of south-southwest declination and moderate negative inclination (Figure 13b) and are interpreted to indicate that the sill acquired a characteristic magnetization during a reversed polarity field.

Interpretation of Paleomagnetic Data

In total, in situ site mean directions from our collection of the Huckleberry Ridge Tuff throughout the Teton-Jackson Hole area show a south-southwest declination and shallow positive inclination strongly suggesting that the area has been tilted about 10° to the west in the past 2.0 m.y. The grand mean of 46 of our in situ site directions (D = 217.6°, I= 6.9°, α_{95}= 7.3° , k= 9.2) is statistically distinct at the 95% confidence level, using the method of *McFadden and Jones* [1981] from two of the three mean directions determined by *Reynolds* [1977] (Figure 13a and Table 5).

We have taken a conservative approach in our comparison because we have included data from several structural settings. For example, a suite of sites along an east-west geologic cross section at the northern end of the Teton Range (Figure 15 and Table 6) shows that in situ site means from the west side of the range are generally consistent with westward tilt. In contrast,

Table 6. Paleomagnetic Data From the Huckleberry Ridge Tuff and Other Igneous Rocks From the Teton Range Area

Site	Locality[a]	n/N/No[b]	D[c]	I[c]	α^{95}[d]	α^{95}[e]1-3	α^{95}[e]1-2	k[f]	Combined[g] (l) and (c)	D	I	α^{95}3-1	α^{95}3-2
TH1	String Creek	8/8/8	246.6	-19.8	9.1	5.3	9.3	38.0					
TH2	String Creek	9/9/10	260.7	-51.2	5.4	3.9	5.3	88.9					
TH4	String Creek	6/6/8	223.2	-12.4	14.7	9.1	13.3	21.8					
TH5	Gran Targhee	7/7/7	196.0	-46.9	4.9	2.9	4.8	148.0					
TH7	Gran Targhee	7/7/7	219.0	13.1	7.4	5.3	6.6	68.2					
TH8	Leigh Creek	5/5/5	208.0	24.0	12.1	3.4	12.0	40.4	5(l), 4(c)	211.2	25.1	6.9	9.9
TH10	Big Hole Mts	10/10/10	213.9	14.0	6.2	1.6	7.5	61.2					
TH11	Big Hole Mts	8/8/8	214.3	-1.4	3.4	1.2	3.8	261.9					
TH12	Big Hole Mts	7/7/7	212.8	5.2	3.9	1.5	4.3	231.6					
TH13	Idaho 32	7/7/7	207.2	-10.4	3.0	2.1	2.7	404.0					
TH14	Conant Creek	8/8/8	210.6	30.7	14.7	3.3	16.7	15.1	8(l), 6(c)	211.0	29.7	8.1	14.6
TH15	Conant Creek	5/5/5	221.1	13.4	19.1	7.2	17.9	17.1	5(l), 5(c)	219.7	11.5	8.6	16.6
TH16	Conant Creek	7/7/7	225.1	19.7	15.3	8.9	15.2	16.4	7(l), 8(c)	221.7	16.4	7.8	15.1
TH17	Grassy Lake	8/8/8	234.9	20.9	21.0	13.5	21.2	7.9	8(l), 8(c)	225.3	15.2	13.0	18.6
TH23	Steamboat Mt	6/6/6	234.5	0.4	14.8	6.4	14.9	21.5	6(l), 5(c)	229.4	5.2	13.1	17.7
TH24	Steamboat Mt	4/4/4	218.7	13.1	10.9	3.1	9.7	71.0	4(l), 8(c)	225.7	20.5	12.7	20.4
TH25	Bailey Creek	10/10/10	228.8	7.7	5.1	3.6	5.1	89.1	10(l), 7(c)	228.7	8.9	3.7	6.0
TH26	Bailey Creek	5/5/5	210.6	8.7	6.6	3.5	5.8	136.5					
TH28	Steamboat Mt	7/7/7	206.7	1.8	9.4	3.2	10.4	41.4					
TH29	Signal Mt	7/7/7	220.5	13.8	8.2	5.1	7.9	54.5	7(l), 6(c)	221.9	14.6	4.8	7.8
TH30	Shadow Mt	10/10/10	197.4	3.5	6.7	4.3	6.9	53.2	10(l), 6(c)	197.1	3.7	4.8	6.6
TH31	Huck Ridge	6/6/6	201.1	-20.5	8.3	4.3	8.0	66.2					
TH32	Huck. Ridge	6/6/6	203.4	-17.3	8.6	4.4	8.4	61.2					
TH33	Huck Ridge	4/4/4	208.3	3.0	6.9	2.6	5.9	175.6	4(l), 5(c)	209.6	2.4	2.8	5.2
TH34	Grassy Lake	8/8/8	216.1	20.5	8.3	6.1	7.6	45.4	8(l), 7(c)	215.2	21.2	6.1	10.5
TH35	Grassy Lake	8/8/8	207.0	-4.4	7.5	5.2	7.1	55.4	8(l), 7(c)	205.2	-4.4	5.4	9.1
TH36	Grassy Lake	7/7/7	240.4	31.3	12.0	5.6	12.6	26.3					
TH36x	Grassy Lake	4/4/4	229.0	-15.0	6.0	0.9	5.5	232.9					
TH37	Steamboat Mt	9/9/9	242.1	-34.0	5.9	1.8	6.9	75.4					
TH38	Signal Mt	7/7/7	196.8	2.3	10.2	2.4	11.4	35.3					
TH39	Signal Mtn	5/5/5	207.3	28.3	12.8	3.1	12.8	36.9	5(l), 3(c)	202.5	32.6	9.1	11.7
TH40	Pilgrim Mt	9/9/9	200.7	20.6	8.5	4.3	9.4	37.2	9(l), 7(c)	202.7	21.1	5.3	8.4
TH41	Pilgrim Mt	9/9/9	214.9	20.2	5.3	4.0	4.9	95.9	9(l), 2(c)	212.3	20.5	5.6	6.8
TH43	Deadman's Bar	10/10/10	206.0	-7.6	2.4	1.7	2.48	404.9					
TH46	Berry Creek	6/6/6	208.3	0.1	8.7	3.5	8.8	60.5					
TH47	Berry Creek	7/7/7	243.6	59.6	16.8	6.9	17.5	13.8					
TH48	Berry Creek	4/4/4	229.0	46.8	18.9	9.1	15.1	24.5	4(l), 4(c)	229.0	43.0	9.3	17.9
TH48x	Berry Creek	4/4/4	203.4	15.9	20.1	7.5	17.3	21.7	4(l), 1(c)	207.1	15.4	14.9	18.6
TH52	Lizard Creek	16/16/16	251.0	4.5	17.6	6.9	10.6	5.3	16(l), 10(c)	245.7	3.7	7.5	10.7
TH57	Berry Creek	8/8/8	213.2	8.1	6.8	2.1	7.8	66.4					
TH61	Conant Creek	10/10/10	214.1	-9.4	3.2	2.2	3.4	227.3					
TH63	Berry Creek	9/9/9	213.	-1.6	2.0	0.8	2.2	654.9					
TH64	Berry Creek	8/8/8	211.4	6.9	3.3			280.6					
TH65	Berry Creek	5/5/5	217.1	-54.2	14.3			29.5					
TH66	Berry Creek	5/5/5	213.3	-3.1	8.4	6.1	6.3	83.2					
TH67	Berry Creek	8/8/8	220.0	3.4	8.4	5.7	8.1	44.3					
TH68	Berry Creek	9/9/9	217.4	-11.3	6.7			59.8					
TH69	Berry Creek	7/7/7	214.9	6.4	3.1			375.9					
TP2	Teton Pass	6/6/6	210.7	-66.3	3.8	2.1	3.6	307.9					
TP3	Teton Pass	6/6/6	224.	-62.8	5.7	3.5	5.2	138.4					
TP4	Teton Pass	9/9/9	200.9	-66.3	4.1	1.9	4.6	153.1					
TP5	Teton Pass	9/9/9	208.	-62.2	6.1	2.3	6.9	72.7					
TP6	Teton Pass	10/10/10	215.7	-61.0	3.4	2.3	3.6	194.3					

[a] Site locations shown on Figure 3.

[b] Number of specimens (n) from number of independently oriented samples used for statistical purposes (N) to the total number of samples (No) collected.

[c] D, declination, and I, inclination of the site or study mean direction of magnetization (in degrees clockwise from north and positive downward), in in situ coordinates.

[d] Semiangle, in degrees, of the 95% cone of confidence about the mean direction.

[e] Bingham statistics [*Onstott*, 1980] both α^{95}1-3 and α^{95}1-2 calculated to assess the non-Fisherian distribution of data about a calculated (in these cases) mean direction.

[f] *Fisher's* [1953] best estimate for the precision parameter of a statistical grouping of N vectors

[g] Results of a combined analysis of stable endpoint (linear) and remagnetization circle (planar) data, with the number of lines (l) and circles (c) used in the analysis indicated. The mean direction is reported along with estimated 95% confidence limits.

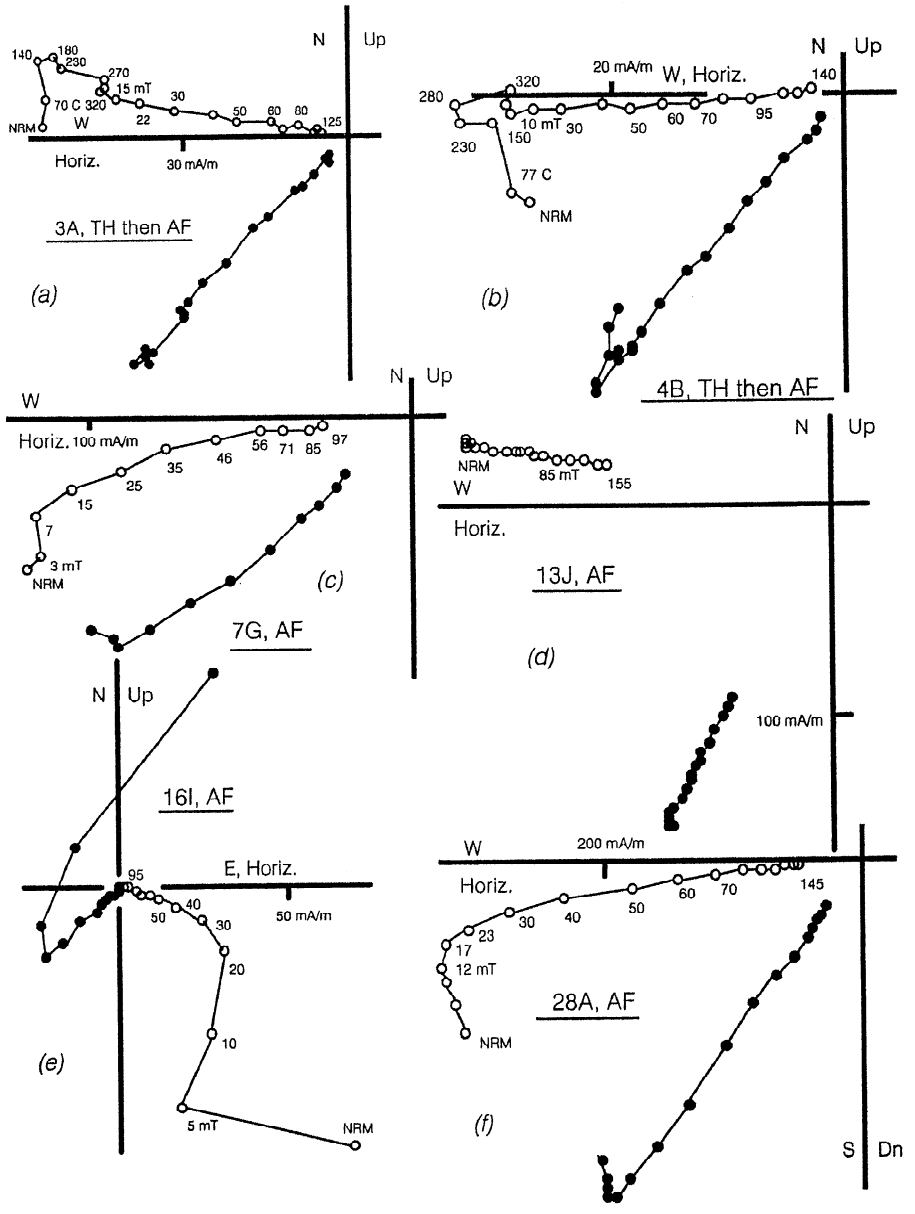

Figure 14. (a)-(h) Examples of response to progressive demagnetization by specimens from samples of the Huckleberry Ridge Tuff and the late Miocene andesite (i) and (j) sill of the Teton Range and surrounding area. Each plot is a modified [*Roy and Park,* 1974] orthogonal demagnetization diagram showing the magnetization vector projected onto the true horizontal plane (solid symbols) and the true vertical plane (vertical component plotted with respect to total horizontal) (open symbols). Demagnetization steps (in milliteslas, (mT) or degrees Celsius) are given along points on the vertical projections.

site means from east of the Teton fault in the structurally complex Steamboat Mountain area do not exhibit a systematic pattern of westward tilt. We note, however, that the inclinations of the western site means vary by up to 17.5° (Table 6), suggesting that the tuff was emplaced on preexisting local topography. Comparison of the sign and magnitude of the inclination of individual site means with the direction and magnitude of dip of eutaxitic structures suggests that overall, the more positive the inclination of a site mean direction, the greater the amount of west dip as recorded by eutaxitic structures (Figure 16). Preexisting topography also complicates this crude relationship. Unfortunately, comparison of hanging wall versus footwall inclinations is precluded by the lack of significant exposures of the Huckleberry Ridge Tuff in the hanging wall of the Teton fault, south of Jackson Lake (Plate 2).

The in situ data from the Teton Pass sill are of southwest declination and moderate negative inclination (D = 212.2, I = -63.9, α_{95} = 4.3°, k = 320.2). It is questionable whether magnetization acquisition in a 20-m-thick sill is capable of averaging secular variation of the geomagnetic field and thus a quantitative comparison between the sill data and an expected late Miocene reverse polarity direction is not appropriate. However, we note that the in situ data from the sill are consistent with a moderate amount (e.g., 10-20°) of west side down tilting since sill emplacement.

The approximately 10° of westward tilt recorded by the Huckleberry Ridge Tuff suggests that significant uplift of the

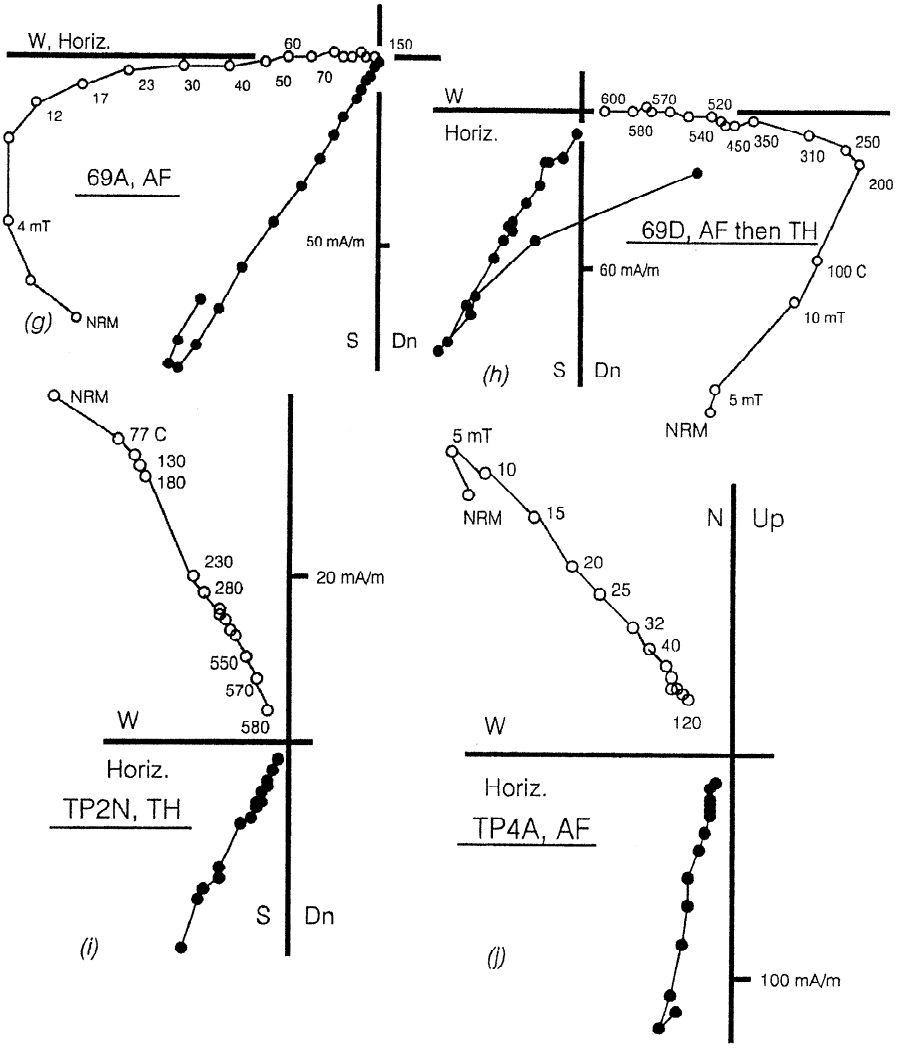

Figure 14. (continued)

Teton Range has occurred in the past 2.0 m.y. However, local deviations in inclination due to emplacement on preexisting topography, coupled with the complex demagnetization behavior, and the anomalous negative inclination of the tuff at a significant number of sites (Table 6) precludes using the paleomagnetic results to rigorously estimate the throw on the Teton fault. Nonetheless the data seem to suggest that the majority of the throw on the Teton fault and development of the Teton Range has occurred during the Quaternary.

Summary

The precipitous eastern range front and overall westward tilt of the Teton Range are dramatic examples of the topographic signature of the long-term history of normal displacement on the active Teton fault. Discrimination of the effects of postglacial fault displacements from the effects of erosion and preexisting structure on the topography of the range is complicated by Laramide deformation of the footwall; however, the pronounced systematic westward tilt of the hanging wall block, Jackson Hole, illustrates the topographic signature of Holocene displacement on the Teton fault.

The systematic pattern of westward tilt of the valley floor of Jackson Hole toward the Teton fault is similar to observations of postseismic and coseismic hanging wall deformation accompanying large ground-rupturing, normal-faulting earthquakes. Boundary element fault models suggest the westward tilt is consistent with accumulated displacement of 110-125 m, producing 10-20 m of footwall uplift along the Teton fault. Comparison of these results with dislocation models of the Borah Peak, Idaho, and Hebgen Lake, Montana, earthquakes suggest that anywhere from 10 to 50 M=7+ earthquakes occurred the Teton fault in the past 25,000-75,000 years. Postglacial surface offsets of up to 38 m preserved in 13,400-17,000 year glacial moraines suggest that much, if not all, of this displacement has accumulated since Pinedale deglaciation. Paleoseismological studies imply, however, that the southern part of the Teton fault has not ruptured in the past 4800 to 7100 years. This suggests that (1) ground-rupturing earthquakes, with displacements comparable to those observed in the trench across the Teton fault, occurred relatively frequently during the 6300-12,000-year interval following Pinedale deglaciation; or (2) earthquakes during this interval were not more frequent, but the their accompanying surface displacements were significantly larger than those observed in the trench.

Integration of gravity and boundary element modeling results suggest the Teton fault dips 60°-75°E. Throw of 2.5-3.5 km has accumulated on the fault since its apparent inception

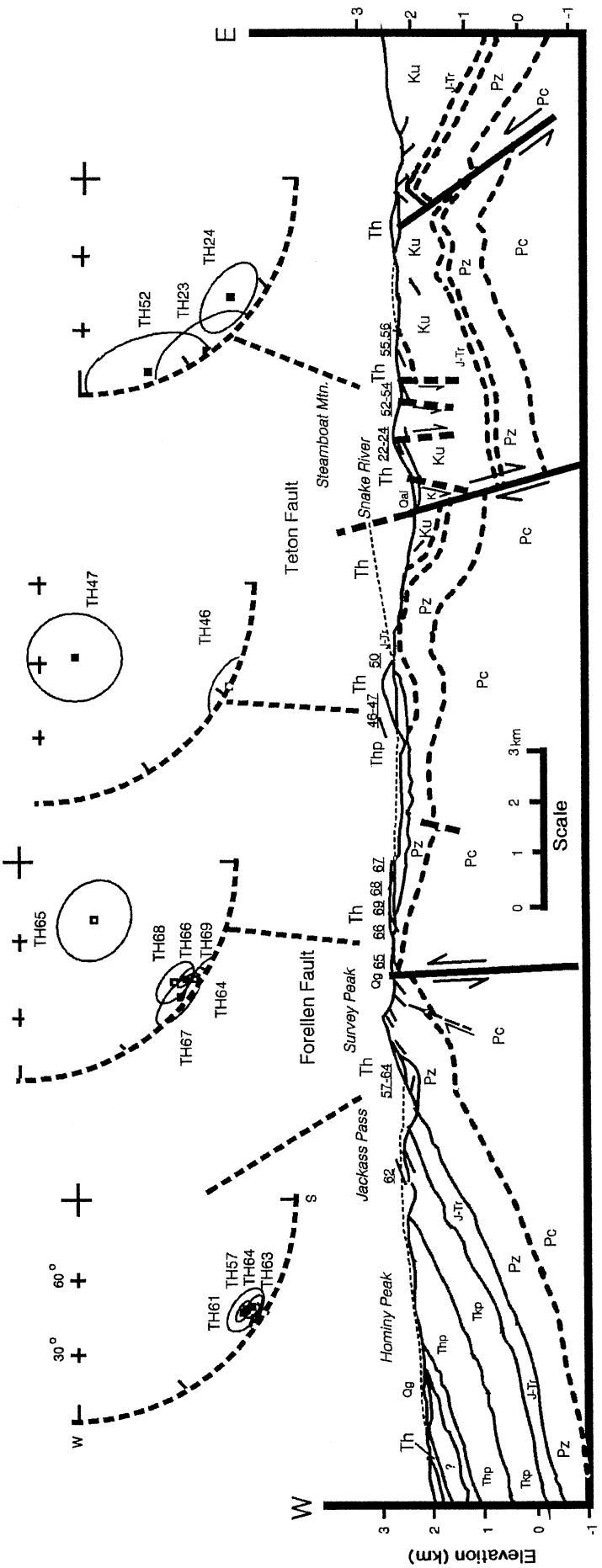

Figure 15. East-west geologic cross section across the northern end of the Teton Range, including equal-area projections of paleomagnetic data from the Huckleberry Ridge Tuff on or near the profile. Geology west of Snake River is from *Christiansen et al.* [1978]; geology east of Snake River is from *Love et al.* [1992]; Teton fault and small normal faults in Steamboat Mountain area are from this study. Each partial equal-area projection shows in situ site mean directions with projected cones of 95% confidence about the mean direction. Cross section location is shown on Figure 3.

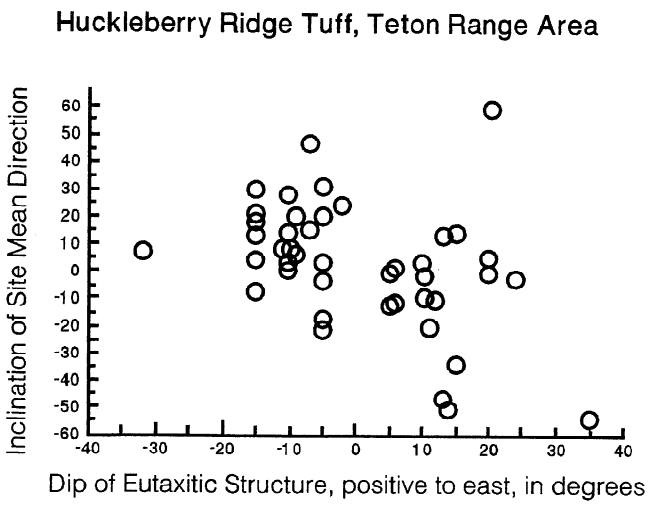

Figure 16. Plot of measured in situ inclinations from sites in the Huckleberry Ridge Tuff versus dip of eutaxitic structures at each site.

possibly 13 Ma, or as recently as 2 Ma. The approximately 10° of postemplacement westward tilt of the Huckleberry Ridge Tuff suggest that much of the displacement on the fault may have occurred place in the past 2 m.y. This implies that if the faulting initiated between 9 and 13 Ma, a relatively minor amount of displacement occurred on the Teton fault throughout the late Miocene. This suggests that the 10°-25°W dips of the Colter and Teewinott formations on the east side of Jackson Hole may actually reflect late Miocene uplift and possible repetition of these units along the western margin of the Gros Ventre and other ranges to the east.

Despite this evidence for significant Quaternary deformation, Laramide and possibly older geologic structures evidently still influence the topographic expression of the Teton Range and Jackson Hole. The high peaks in the central part of the Teton Range appear to have been uplifted on a high angle Laramide reverse fault, and our gravity modeling suggests a similar structure, which displaced relatively high density rocks, may have been offset across the northern and central parts of the Teton fault. This preextensional high-density feature may partially control the apparent location of the northern hanging wall basin depocenter, 10 km east of the Teton fault. In contrast, the gravity models suggest the southern part of the Teton fault does not displace a high-density body, and the southern hanging wall basin depocenter is in a more characteristic position, 4 km east of the fault trace. These long-lived influences on the spectacular topography of the Teton Range illustrate the pitfall of ascribing variations in normal fault footwall topography simply to normal fault kinematics.

Acknowledgments. This paper presents the principal findings of a multifaceted research project focused on the seismotectonics and earthquake hazards of the Grand Teton National Park and the Teton fault. It was primarily funded by the University of Wyoming-National Park Service Research Center, grant 532724. Funds for the general seismotectonic studies were provided by the U.S. Geological Survey, National Earthquake Hazards Reduction Program grants 14-08-00001-G1349. The Wyoming Geological Survey also provided partial support for field efforts. We gratefully acknowledge the cooperation of the Grand Teton National Park staff including the superintendent, Jack Stark, and other staff members; Marshall Gingery, Peter Hayden, and Patrick Smith. Geoffrey King, IGP Straussborg University, kindly made his boundary element program available. His insights on the mechanics and geologic aspects of normal faulting were an invaluable contribution to our work. B. Hardman, B. Horton, S. Harlan, C. Ratcliff, C. DeWolf, and M. Liss assisted with the paleomagnetic field sampling and analyses. M. Steadman, J. Helm, and B. Palmer assisted with the topographic profiling and gravity surveys. The University of Utah provided support for computing. W. Bonini and P. Lavin provided gravity data and contributed copies of original figures. Vicki Bankey also provided regional gravity data, and processed the gravity data and made terrain corrections for our gravity surveys. We also thank Jack Shea of the Teton Science School for providing housing and logistical support during part of our field work. Art Sylvester, Tony Lowry, Dean Ostenaa, Ron Bruhn, and J. David Love gave helpful advice and discussions throughout our project. Reviews by E. Duebendorfer, M. Ellis, and W. Taylor led to a greatly improved manuscript. Support for reproduction of color plates has been provided by NASA Grant 3338 to Michael A. Ellis.

References

Anders, M.R., J.W. Geissman, L.A. Peity, and J.T. Sullivan, Parabolic distribution of circumeastern Snake River Plain seismicity and latest Quaternary faulting: Migratory pattern and association with the Yellowstone Hotspot, *J. Geophys. Res., 94,* 1589-1621, 1989.

Barnosky, A.D., The Colter Formation: Evidence for Miocene volcanism in Jackson Hole, Teton County, Wyoming, *Wy. Geol. Assoc. Earth Sci. Bull. 16,* 50-101, 1984.

Barrientos, S.E., R.S. Stein, and S.N. Ward, Comparison of the 1959 Hebgen Lake, Montana and the 1983 Borah Peak, Idaho earthquakes from geodetic observations, *Bull. Seismol. Soc. Am., 77,* 784-808, 1987.

Behrendt, J.S., B.L. Tibbetts, W.E. Bonini, and P.M. Lavin, A geophysical study in Grand Teton National Park and vicinity, Teton County, Wyoming, *U.S. Geol. Surv. Prof. Pap., 516-E,* 23 pp., 1968.

Blackwelder, E., Post-Cretaceous history of the mountains of central western Wyoming, *J. Geol., 23,* 193-217, 1915.

Bonilla, M.G., R.K. Mark, and J.J. Lienkaemper, Statistical relations among earthquake magnitude, surface rupture length, and surface fault displacement, *Bull. Seismol. Soc. Am., 74,* 2379-2411, 1984.

Byrd, J. O. D., Paleoseismicity of the southern section of the Teton fault, Wyoming, *Geol. Soc. Am. Abstr. Programs, 23,* A481, 1991.

Byrd, J.O.D., Neotectonics of the Teton fault, Wyoming,Univ. of Utah, Ph.D. dissertation, 295 p., Salt Lake City, 1994.

Byrd, J.O.D., J. W. Geissman, and R.B. Smith, Seismotectonics of the Teton fault and possible relationship to the Yellowstone Hotspot, *Eos Trans. AGU, 69,* 1419, 1988.

Christiansen, R.L., Late Cenozoic volcanism of the Island Park area, eastern Idaho, in Cenozoic Geology of Idaho, edited by B. Bonnichsen and R.M. Breckenridge, Idaho Bur. Mines Geol. Bull. 26, 345-368, 1982

Christiansen, R.L., H.R. Blank, Jr., J.D. Love, and J.C. Reed, Jr., Geologic map of the Grassy Lake Reservoir Quadrangle, Yellowstone National Park and vicinity, Wyoming, scale 1:62,500, *U.S. Geol. Surv. Geol. Quad. Map, GQ-1459,* 1978.

Coe, R.S., and M. Prevot, Evidence suggesting extremely rapid field variation during a geomagnetic reversal, *Earth Planet. Sci. Letts., 92,* 292- 298, 1992.

Crone, A.J., and M. Machette, Surface faulting accompanying the Borah Peak earthquake, central Idaho, *Geology, 12,* 664-667, 1984.

Crouch, S.L., and A.M. Starfield, *Boundary Element Methods in Solid Mechanics,* 322 pp., Allen and Unwin, Winchester, Mass., 1983.

Doser, D.I., and R.B. Smith, Seismicity of the Teton-Southern Yellowstone region, Wyoming, *Bull. Seismol. Soc. Am., 73,* 1369-1394, 1983.

Edmund, R.W., Structural geology and physiography of the northern

end of the Teton Range, Wyoming, *Augustana Lib. Publ. 23*, 81 pp., 1951.

Ellis, M., and G.C.P. King, Structural control of flank volcanism in continental rifts, *Science, 254*, 839-842, 1991.

Fisher, R.A., Dispersion on a sphere, *Proc. R. Soc. London, Ser. A, 217*, 295-305, 1953.

Fryxell, F. M., Glacial features of Jackson Hole, *Augustana Lib. Publ. 13*, 55 pp., 1930.

Fryxell, F. M., Postglacial faulting in the Teton Range, Wyoming, *Geol. Soc. Am. Bull., 49*, 1881, 1938.

Fryxell, F.M., L. Horberg, and R. Edmund, Geomorphology of the Teton Range and adjacent basins, Wyoming-Idaho (abstract), *Geol. Soc. Am. Bull. 52*, 1903, 1941.

Geissman, J.W., M. Jackson, A.S. Harlan, and R. Van der Voo, Paleomagnetism of latest Cambrian-Early Ordovician and latest Cretaceous-early Tertiary rocks of the Florida Mountains, southwest new Mexico, *J. Geophys. Res., 96*, 6053-6071, 1991.

Gilbert, J. D., D. Ostenaa, and C. Wood, Seismotectonic study Jackson Lake Dam and Reservoir, Minidoka Project, Idaho-Wyoming, 123 pp., *Seismotectonic Rep. 83-8*, U.S. Bur. of Reclam., Boise, Idaho, 1983.

Horberg, L., V. Nelson, and V. Church, Structural trends in central western Wyoming, *Geol. Soc. Am. Bull., 60*, 183-216, 1949.

Horberg, L., R.W. Edmund, and F.M. Fryxell, Geomorphic and structural relations of Tertiary volcanics in the northern Teton Range and Jackson Hole, Wyoming, *J. Geol., 63*, 501-511, 1955.

King, G. C. P., Speculations on the geometry of the initiation and termination processes of earthquake rupture and its relation to morphology and geological structure, *Pure Appl. Geophys., 124*, 567-585, 1986.

King, G. C. P., and M. Ellis, The origin of large local uplift in extensional regions, *Nature, 348*, 689-693, 1990.

King, G. C. P., and J. Nabelek, Role of fault bends in the initiation and termination of earthquake rupture, *Science, 228*, 984-987, 1985.

King, G. C. P., R. S. Stein, and J. B. Rundle, The growth of geological structures by repeated earthquakes, 1, Conceptual framework, *J. Geophys. Res., 93*, 307-318, 1988.

Kirschvink, J. L., The least-squares line and plane and the analysis of palaeomagnetic data, *Geophys. J. R. Astron. Soc., 62*, 699-718, 1980.

Lageson, D. R., Possible Laramide influence on the Teton normal fault, western Wyoming, in Regional Geology of Eastern Idaho and Western Wyoming, edited by P.K. Link, M. A. Kuntz, and L. B. Platt, *Mem. Geol. Soc. Am., 179*, 183-195, 1992.

Lavin, P.M., Detailed gravity measurements in the Jackson Hole-Teton Mountains area of northwestern Wyoming, 46 pp., B.S.E. thesis, Princeton Univ., Princeton, N.J., 1957.

Lavin, P.M., and W.E. Bonini, Detailed gravity measurements in the Teton Range and Jackson Hole, Wyoming, *Geol. Soc. Am. Bull., 68*, 1760, 1957.

Love, J.D., Summary of Upper Cretaceous and Cenozoic stratigraphy, and of tectonic and glacial events in Jackson Hole, northwestern Wyoming, *Guideb. Wyo. Geol. Assoc. Annu. Field Conf., 29th*, 585-593, 1977.

Love, J.D., Teton mountain front, Wyoming, in *Geological Society of America Centennial Field Guide*, pp. 173-178, Geologic Society of America, Rocky Mountain Section, Golden, Colo., 1987.

Love, J.D., and H.F. Albee, Geologic map of the Jackson Quadrangle, Teton County, Wyoming, scale 1:24,000,*U.S. Geol. Surv. Map I-769A*, 1972.

Love, J.D., and J. de la Montagne, Pleistocene and Recent tilting of Jackson Hole, Teton County, Wyoming,*Guideb. Wyo. Geol. Assoc. Annu. Field Conf., 11th*,1 69-178, 1956.

Love, J.D., and J.C. Reed, Jr., *Creation of the Teton Landscape, the Geological Story of Grand Teton National Park*, 120 pp., Grand Teton Natural History Association, Moose, Wyo., 1971.

Love, J.D., J.C. Reed Jr., R.L. Christiansen, and J.R. Stacy, Geologic block diagram and tectonic history of the Teton region, Wyoming-Idaho, *U.S. Geol. Surv. Misc. Invest. Ser., Map I-730*, 1973.

Love, J.D., J.C. Reed Jr., and A.C. Christiansen, Geologic map of Grand Teton National Park, Teton County, Wyoming, scale 1:62,500, *U.S. Geol. Surv. Misc. Invest. Ser., Map I-2031*, 1992.

McFadden, P.L., and F.J. Lowes, The discrimination of mean directions drawn from Fisher distributions, *Geophys. J. R. Astron. Soc., 67*, 19-33, 1981.

Machette, M. N., S.F. Personius, A.R. Nelson, D.P. Schwartz, and W. R. Lund, The Wasatch fault zone, Utah-Segmentation and history of earthquakes, *J. Struct. Geol., 13*, 137-149, 1991.

Mankinen, E.A., E.E. Larson, C. S. Gromme, M. Prevot, and R.S. Coe, The Steens Mountain (Oregon) geomagnetic polarity transition, 3, Its regional significance, *J. Geophys. Res., 92*, 8057-8076, 1987.

Morgan, L.A., Stratigraphic relations and paleomagnetic and geochemical correlation of ignimbrites of the Heise volcanic field, eastern Snake River Plain, eastern Idaho and western Wyoming, in Regional Geology of eastern Idaho and Western Wyoming, edited by P.K. Link, M.A. Kuntz, and L.B. Platt, *Mem. Geol. Soc. Am. 179*, 215-226, 1992.

Onstott, T.C., Applications of the Bingham distribution function in paleomagnetic studies, *J. Geophys. Res., 85*, 1500-1510, 1980.

Ostenaa, D.A., Late Quaternary behavior of the Teton fault, Wyoming, *Geol. Soc. Am. Abstr. Programs, 20*, A14, 1988.

Pierce, K. L., and J. Good, Quaternary geology of Jackson Hole, Wyoming, in Geologic Field Tours of Western Wyoming and parts of adjacent Idaho, Montana, and Utah, edited by S. Roberts, *Pub. Info. Circ. 29*, pp. 79-88, Geol. Surv. of Wyo., Laramie, 1990.

Reed, J. C., and A.E. Zartman, Geochronology of Precambrian rocks of the Teton Range, *Geol. Soc. Am. Bull., 84*, 561-582, 1973.

Reynolds, R.L., Paleomagnetism of welded tuffs of the Yellowstone Group, *J. Geophys. Res., 82*, 3677-3693, 1977.

Roberts, S.V., and D.W. Burbank, Uplift and thermal history of the Teton Range defined by apatite fission-track dating, northwestern Wyoming, *Earth Planet. Sci. Lett., 118*, 295-309, 1993.

Roy, J. L., and J. K. Park, The magnetisation process of certain red beds: Vector analysis of chemical and thermal results, *Can. J. Earth Sci., 11*, 437-471, 1974.

Royse, F., Jr., Extensional faults and folds in the foreland thrust belt, Utah, Wyoming, Idaho, *Geol. Soc. Am. Abstr. Programs, 15*, 295, 1983.

St. John, O., Report of the geological field work of the Teton division, U.S. Geologic Geographic Survey Territory, in 11th Annual Report, pp. 321-508, U.S. Geol. Surv., Reston, Va., 1879.

Sales, J. K., Collapse of Rocky Mountain foreland uplifts, in *Rocky Mountain Foreland Basins and Uplifts*, edited by J.D. Lowell, pp. 79-97, Rocky Mountain Association of Geologists, Denver, Colo.,1983.

Sarna-Wojciciki, A.M., and M.S. Pringle Jr., Laser-fustion $^{40}Ar/^{39}Ar$ ages of the Tuff of Taylor Canyon and Bishop Tuff, E. California-W. Nevada, *Eos Trans. AGU, 73* (43) Fall Meeting suppl., 633, 1992.

Schwartz, D. P., and K. J. Coppersmith, Fault behavior and characteristic earthquakes; Examples from the Wasatch and San Andreas fault zones, *J. Geophys. Res., 89*, 5681-5698, 1984.

Shuey, R.T., R.O. Ugland, and C.R. Schmidt, Magnetic properties and secular variation in cores from Yellowstone and Jackson Lakes, Wyoming, *J. Geophys. Res., 82*, 3739-3746, 1977.

Smith, D.J., Structural analysis of the Buck Mountain fault and related intra-range faults, Teton Range, Wyoming, Master's thesis, 92 pp., Mont. State Univ., Bozeman, 1991.

Smith, R.B., and W.J. Arabasz, Seismicity of the Intermountain Seismic Belt, in *Neotectonics of North America*, Decade Map vol. 1, edited by D.B. Slemmons, E.R. Engdahl, M.D. Zoback, and D.D. Blackwell, pp. 185-228, Geological Society of America, Boulder, Colo., 1991.

Smith, R.B., J.R. Pelton, and J.D. Love, Seismicity and the possibility of earthquake related landslides in the Teton-Gros Ventre-Jackson Hole area, Wyoming, *Contrib. Wyo. Geol., 14*, 57-64, 1977.

Smith, R. B., J. O. D. Byrd, and D. D. Susong, Neotectonics and structural evolution of the Teton fault, in Geologic Field Tours of

Western Wyoming and parts of adjacent Idaho, Montana, and Utah, edited by S. Roberts, *Pub. Info. Circ. 29*, pp. 126-138, Geol. Surv. of Wyo., Laramie, 1990.

Smith, R.B., J.O.D. Byrd, and D.D. Susong, Seismotectonics, Quaternary history, and earthquake hazards of the Teton fault, Wyoming, in *Geology of Wyoming, Mem. 5*, edited by A. Snoke, J.R. Steitdmann, and S. Roberts, pp. 628-667, Geologic Survey of Wyoming, Laramie, 1993a.

Smith, R.B., K. L. Pierce, and R.J. Wold, Seismic Surveys and Quaternary History of Jackson Lake, Wyoming, in *Geology of Wyoming, Mem. 5*, edited by A. Snoke, J.R. Steitdmann, and S. Roberts, pp. 668-693, Geologic Survey of Wyoming, Laramie, 1993b.

Stuiver, M., and P.J. Reimer, Extended ^{14}C data base and revised CALIB 3.0 ^{14}C age calibration program, *Radiocarbon, 35*, 215-230, 1993.

Susong, D.D., R.B. Smith, and R.L. Bruhn, Quaternary faulting and segmentation of the Teton fault zone, Grand Teton National Park, Wyoming, *Eos Trans. AGU, 68*, 1452, 1987.

Sylvester, A. G., J. O. D. Byrd, and R. B. Smith, Geodetic evidence for aseismic reverse creep across the Teton normal fault, *Geophys. Res. Lett., 18*, 1083-1086, 1991.

Tibbetts, B.L., J.C. Behrendt, and J.D. Love, Seismic-refraction measurements in Jackson Hole, Wyoming, *Geol. Soc. Am. Bull., 80*, 1109-1122, 1969.

Whitlock, C., Postglacial Vegetation and Climatic of Grand Teton National Park and southern Yellowstone National Park, Wyoming: *Ecol. Mono., 63*, 173-198, 1993.

Zelt, C.A., and R.B. Smith, Seismic travel time inversion for 2-D crustal velocity structure, *Geophys. J. Int., 108*, 16-34, 1992.

J.O.D. Byrd, Exxon Production Research Company, MS N-102, P.O. Box 2189, Houston, TX 77252-2189.

J.W. Geissman, Department of Earth and Planetary Sciences, University of New Mexico, Albuquerque, NM 87131.

R.B. Smith, Department of Geology and Geophysics, University of Utah, Salt Lake City, UT 84112.

(Received April 23, 1993; revised December 27, 1993;
accepted January 28, 1994.)